การศึกษาออกแบบสเปกโตรมิเตอร์สำหรับการวัดการแผ่รังสีเอกซ์พลังงานต่ำ

นายนฤดม นวลขาว

วิทยานิพนธ์นี้เป็นส่วนหนึ่งของการศึกษาตามหลักสูตรปริญญาวิทยาศาสตรมหาบัณฑิต
สาขาวิชาฟิสิกส์
มหาวิทยาลัยเทคโนโลยีสุรนารี
ปีการศึกษา 2543
ISBN 974-7359-63-4

DESIGN STUDY OF SOFT X-RAY EMISSION SPECTROMETER

MR. NARUDOM NOULKHOW

A Thesis Submitted in Partial Fulfillment of the Requirements

for the Degree of Master of Science in Physics

Suranaree University of Technology

Academic Year 2000

ISBN 974-7359-63-4

Thesis Title

Design Study of Soft x-ray Emission Spectrometer

Suranaree University of Technology Council has approved this thesis submitted in partial fulfillment of the requirements for a Master's Degree.

Thesis Examining Committee

……..
(Assoc. Prof. Dr. Prasart Suebka)
Chairman

……..
(Dr. Prayoon Songsiriritthigul)
Thesis Advisor

……..
(Prof. Dr. Takehiko Ishii)
Member

……..
(Dr. B.N. Raja Sekhar)
Member

……...
(Dr. Saroj Rujirawat)
Member

…… ……
(Assoc. Prof. Dr. Kasem Prabriputaloong) (Assoc. Prof. Dr. Tassanee Sukosol)
Vice Rector for Academic Affairs Dean, Institute of Science

นายนฤดม นวลขาว: การศึกษาออกแบบสเปกโตรมิเตอร์สำหรับการวัดการแผ่รังสีเอกซ์พลังงานต่ำ
(DESIGN STUDY OF SOFT X-RAY EMISSION SPECTROMETER)
อ. ที่ปรึกษา: ดร. ประยูร ส่งสิริฤทธิกุล, 92 หน้า. ISBN 974-7359-63-4

เทคนิคการศึกษาสเปกตรัมการแผ่ของรังสีเอกซ์พลังงานต่ำเป็นการวัดความเข้มและพลังงานของโฟตอนที่แผ่ออกจากอิเล็กตรอนที่ถูกกระตุ้นโดยโฟตอนหรืออิเล็กตรอน เทคนิคดังกล่าวมีประโยชน์มากในการศึกษาโครงสร้างเชิงอิเล็กทรอนิกส์ของสสาร ในกรณีตัวอย่างที่ทำการศึกษาเป็นของแข็ง ค่าความลึกที่รังสีเอกซ์พลังงานต่ำสามารถทะลุผ่านได้อาจมีค่าถึง 100 นาโนเมตร การใช้แสงซินโครตรอนที่มีความเข้มของแสงสูงมาเป็นตัวกระตุ้นอิเล็กตรอนภายในสสารจะช่วยแก้ไขปัญหาที่เกิดจากปริมาณรังสีเอกซ์พลังงานต่ำที่ถูกปลดปล่อยออกมามีค่าน้อย โดยเฉพาะอย่างยิ่งในกรณีที่ตัวอย่างที่ทำการศึกษาเป็นธาตุที่มีเลขอะตอมน้อยๆ ซึ่งโดยทั่วไปสัดส่วนของจำนวนโฟตอนที่ปลดปล่อยออกมาต่อจำนวนโฟตอนที่ใช้ในการกระตุ้นมีค่าประมาณ 0.1 % นอกจากนี้ สเปกโตรมิเตอร์ที่มีความสามารถในการแยกแยะสูงเป็นที่ต้องการในการที่ใช้วัดและบ่งบอกถึงความแตกต่างของโฟตอนที่ปลดปล่อยออกมาจากอะตอมของธาตุใดธาตุหนึ่งที่ถูกกระตุ้นแต่อยู่ในสภาวะที่ล้อมรอบด้วยธาตุชนิดที่แตกต่างกันได้ หรือใช้ในการบ่งบอกถึงความแตกต่างของสปิน (Spin) ของอิเล็กตรอนที่อยู่ในชั้นระดับพลังงานเดียวกัน ในปัจจุบันมีเพียงสเปกโตรมิเตอร์ที่มีความสามารถในการแยกแยะสูงรูปแบบเดียวที่ผลิตขึ้นในเชิงการค้า โดยบริษัท Gammadata ประเทศสวีเดน

วัตถุประสงค์ของวิทยานิพนธ์จึงมุ่งเน้นไปที่การออกแบบสเปกโตรมิเตอร์ของรังสีเอกซ์พลังงานต่ำที่มีกำลังในการแยกสูงเทียบเท่าหรือสูงกว่าสเปกโตรมิเตอร์ที่ผลิตขึ้นโดยบริษัท Gammadata ในการศึกษาออกแบบเริ่มต้นจากการประเมินเพื่อกำหนดหลักเกณฑ์ที่ใช้ในการออกแบบ เช่น ช่วงพลังงาน ความสามารถในการแยกแยะ ค่าฟลักซ์ ค่าตัวแปรทางทัศนศาสตร์ของสเปกโตรมิเตอร์ และขนาดของส่วนประกอบที่เป็นอุปกรณ์ทางทัศนศาสตร์ รวมถึงความเป็นไปได้ในการจัดหาอุปกรณ์ดังกล่าว จากนั้นจึงทำการประเมินค่าประสิทธิผล ค่าการส่งผ่าน และ กำลังในการแยกของสเปกโตรมิเตอร์โดยอาศัยวิธีการวิเคราะห์ด้วยสมการทางคณิตศาสตร์ ในขั้นตอนสุดท้ายเป็นการใช้โปรแกรม RAY เพื่อจำลองการทำงานของระบบทัศนศาสตร์ของสเปกโตรมิเตอร์โดยใช้ค่าตัวแปรต่าง ๆ ทางทัศนศาสตร์ที่หาได้จากขั้นตอนที่สอง งานวิทยานิพนธ์ฉบับนี้ได้อธิบายถึงรายละเอียดของการคำนวณค่าตัวแปรต่างๆของระบบทัศนศาสตร์ของสเปกโตรมิเตอร์และผลการประเมินประสิทธิภาพการทำงานของสเปกโตรมิเตอร์

สาขาวิชาฟิสิกส์ ลายมือนักศึกษา……..……...…..
ปีการศึกษา 2543 ลายมืออาจารย์ที่ปรึกษา……..……..……
ลายมืออาจารย์ที่ปรึกษาร่วม……...…….. …
ลายมืออาจารย์ที่ปรึกษาร่วม……..……..…….

MR. NARUDOM NOULKHOW: DESIGN STUDY OF SOFT X-RAY EMISSION SPECTROMETER, THESIS ADVISOR: PRAYOON SONGSIRIRITTIGUL, Ph.D. 92 PP. ISBN 974-7359-63-4

The measurement of intensity and energy of the emitted photons consequent of electron or photon excitation known as soft X-ray emission spectroscopy, is a very useful method to study various electronic structure problems. In the case of solids, the penetration depth of soft X-ray could be as large as 100 nanometer. The very low fluorescence yield for soft X-ray, typically about 0.1% for low atomic numbers was an obstacle for soft X-ray emission spectroscopy prior to the development of the extremely intense synchrotron radiation sources. A high resolving power spectrometer is required to measure the emissions from the excitation of chemically shifted species or to separate spin-orbit component in an emission spectrum. At present, there is only one existing commercial model for a high resolving power commercially available soft X-ray emission spectrometer, supplied by Gammadata (Sweden).

The aim of this thesis is to design a high resolving power soft X-ray emission spectrometer with compatible or better performance than the existing commercial spectrometer. The procedure to achieve the goals has been done in many steps. To start with using the design criteria such as energy range, resolving power, flux, size, and the availability of optical components, the optical parameters of the spectrometer required were evaluated. In the second step, the first order evaluation of the spectrometer for efficiency, transmission and resolution was performed using analytical equations. In the third step, by using the optical parameters, the detailed evaluation of the optical performance of the spectrometer has been carried out by means of exact ray tracing. In this thesis, the details of the calculation of the optical parameters, and the result from the ray tracing simulations are described.

ÊÒ¢ÒÇÔªÒ¿ÔÊÔ¡Êì	ÅÒÂÁ×Íª×èÍ¹Ñ¡ÈÖ¡ÉÒ..
»Õ¡ÒÃÈÖ¡ÉÒ 2543	ÅÒÂÁ×Íª×èÍÍÒ¨ÒÃÂì·Õè»ÃÖ¡ÉÒ......................................
	ÅÒÂÁ×Íª×èÍÍÒ¨ÒÃÂì·Õè»ÃÖ¡ÉÒÃèÇÁ.................................
	ÅÒÂÁ×Íª×èÍÍÒ¨ÒÃÂì·Õè»ÃÖ¡ÉÒÃèÇÁ.................................

Acknowledgements

I wish to express my deepest gratitude to my thesis advisor, Dr. Prayoon Songsiriritthigul for his guidance, support, constructive comments and encouragement thoughout the course of my study. His kindness will always be remembered.

I wish to thank Dr. B.N. Raja Sekhar for his help, suggestions and corrections regarding my thesis. The work presented in this thesis is possible only with the help of ray tracing program provided by Dr. Franz Schäfers, BESSY (Germany).

I am thankful to NSRC staffs especially scientists and engineers in the Beamline division for their help. I'm extremely happy to work with them. I am very much helped in improving my knowledge by the lectures in School of Physics.

Finally, I am most grateful to my parents and my brother for their continuous encouragement, constant care and assistance during the course of work.

Narudom Noulkhow

Contents

page

Contents (Continued)

Page

Contents (Continued)

Page

List of Tables

Table **Page**

List of Figures

Figure **Page**

List of Figures (Continued)

Figure **Page**

List of Figures (Continued)

Figure **Page**

List of Figures (Continued)

Figure **Page**

Chapter I

Introduction

1.1. Soft X-ray Emission Spectroscopy

Soft X–ray emission spectroscopy (SXES) is one of the important and useful tools for the study in atomic, molecular and solid structures. The photon or electron excitation fluorescence yield for soft x-rays is very low. Typical yield is about 0.1% for low atomic numbers and which was an obstacle for performing soft x-ray emission spectroscopy experiments historically. Because of the development of synchrorton light sources that can produce high intense photon flux, it is possible to compensate the low fluorescence yield. For example, the Siam Photon Source [Songsiriritthigul, Pairsuwan, Jearanaikoon, and Ishii, 1999] with undulator can produce synchrotron light with brightness as high as 10^{17} photons/s/mrad^2/0.1%BW at 200mA of electron current. In the recent years, SXES has increasingly been used to obtain very good experimental results in many synchrotron radiation research facilities. Some of the important applications of SXES, especially using synchrotron light sources are described in the following paragraphs.

The ability to monochromatize light from Synchrotron light sources with any wavelength and with very narrow bandpass allow one to excite an individual close lying core state. If a high resolving power spectrometer is employed to measure the emission from the excitation, chemically shifted species or spin-orbit component can be separated in the emission spectrum [Wiell, 1995]. Invaluable information of electronic structures can thus be deduced from the measurement.

Modern high brightness synchrotron radiation sources have helped SXES to become a potent method for various structure problems, which were previously not accessible for this method [Nordgren, 1996]. The inherently selective properties of soft X-ray emission (SXE), which probe localization and angular momentum of

valence electrons, can now be fully exploited. Due to the penetration properties of soft X-rays, both surface overlayers [Wassdahl, et.al., 1992; Tillborg, et.al., 1993; Nilsson, et.al., 1995] and buried systems [Nilsson, et.al., 1995; Perera, Zhang, Calicott, and Ederer, 1989; Carlisle, et.al., 1995] as well as true bulk properties of materials can be studied. In particular gaseous molecules lend themselves to studies in resonant soft X-ray emission.

The ability to tune the excitation to narrow bandpass allows one to discriminate between close lying core excited states, and thereby to separate e.g. chemically shifted species or spin-orbit components in the emission spectrum. In this way, different sites in a compound system can be studied with regard to local electronic structure, i.e., it different oxygen sites in a high temperature superconductor [Guo, et.al., 1994; Butorin, et.al., 1995; Butorin, et.al., 1994; Guo, et.al, 1993] or the different atoms of a molecule adsorbed on a metal surface [Wiell, 1995; Nilsson, et.al., 1995].

Considering the resonantly exited SXES, one often needs to apply a resonant inelastic scattering picture [Aberg and Crasemann, 1994; Gelmukhanov, Mazalov and Shkiyaeva, 1976]. This is true in particular when the intermediate core exited state is degenerate or quasi-degenerate, and thus enable the interference effect. Resonant X-ray fluorescence processes invoke two-photon symmetry selection rule which govern the absorption and emission processes, and thus provide a mean to relate the symmetry of the absorption state to that of the emission state [Gel'mukhanov and Agren, 1994]. Dynamical symmetry breaking occurring on the time scale of the core state lifetime (femto-seconds) can be studied by virtue of the symmetry dependence of the X-ray emission intensities through selection rules [Skytt, et.al., 1996].

Polarization and anisotropy of X-ray emission can be used to study orbital components, bond directions and molecular orbital symmetries. The use of monochromatized synchrotron radiation allows non-ordered systems, including molecules in the gas phase, to be studied by X-ray emission with respect to angular distributions. This is because of the fact that the excitation provides alignment with respect to the direction of the polarization, and this alignment is preserved throughout the absorption/emission process [Lindle, et.al., 1988; Southworth, Lindle, Meyery, and Cowan, 1991].

The wonderful performance of SXES experiments described above require the availability of high flux and high-resolution soft X-ray monochromator/ spectrometers. Apart from the fact that low yields associated with the emission of soft X-rays prevent the full exploitation of soft X-ray emission spectroscopy, the comparatively small solid angles of acceptance of grating instruments needed for high resolution recording of spectra in the low energy range has mounted further obstacles. The introduction of synchrotron radiation in the 1970's immediately promoted the development of other electronic spectroscopies. However, it did not have a prompt impact on soft X-ray emission studies, since the performance of beamlines at that time did not allow monochromatized radiation of sufficient intensity to be used for the excitation. Only when undulator sources had come into operation and more efficient grating instruments had been developed one could start to perform studies of selectively excited soft X-ray emission [Rubensson, et.al., 1988]. With energy selectivity in the excitation one could attain a long standing goal, to separate X-ray satellites due to multiple excitations, which notoriously obscured the analysis of broad band excited X-ray band spectra. Also, one could study resonant effects in emission spectra, which subsequently led to new insights and opened new pathways to study electronic structures and dynamics.

The third generation synchrotron radiation sources have contributed to put the present spectroscopy alongside with other established synchrotron radiation spectroscopies with feasibility and freedom of choices of systems to study. Normally, fluxes of the order of 10^{12}-10^{13} photons per second in < 0.1% bandpass and < 0.1 mm focused beam heights are provided at beamlines adapted to the sources [Warwick, Heimann, Mossessain, and Padniore, 1995]. These are the typical numbers required to allow the measurements on convenient time scales, also for diluted systems like monolayer adsorbates.

Although a trivial fact, it is interesting to point out that the pursuit of soft X-ray fluorescence studies is largely depended on the brightness of the source. Obviously the small angular acceptance of grazing incidence grating spectrometers are badly matched to all but low emittance sources, and the most efficient way to attain best matching is to produce a small spot of exciting radiation on the sample. The spatial resolution of available area detectors for soft X-rays (even for grazing

incidence mounting) is often a factor that limit the spectral resolution. Typically, several thousandth in resolving power is obtained in small and medium size grazing incidence instruments provided with entrance slits of matching width (with respect to detector resolution), which means typically one or two hundredth of a millimeter. (This is a number which approximately also matches the lifetime broadening of the core excited states.) It is easily realized that one can gain, in sensitivity, by diminishing the source size to approach these measures. The well defined polarization of synchrotron radiation offers a mean to obtain more detailed information in many spectroscopies, so also for soft X-ray fluorescence. However, due to their sizes and weights, conventional spectrometers for soft X-ray emission do not readily lend themselves for mounting in rotating configurations, which is desired in order to study the angular dependence of the emission with respect to the exciting radiation polarization.

1.2. History of Soft X-ray Spectrometers

In 1930's electron beam excited soft x-ray emission spectroscopy using grating spectrometers was pioneered by T.H. Osgood [1933], M. Sigbahn [1937] and H.W.B. Skinner [1940] and was actively pursued by many scientists though the 1950s. The review articles by Tomboulian [1957] and Parratt [1959] devoted mostly to light elements and light element compounds from the second and third rows of the periodic table. In the late 1960's SXES experiments were performed using Seya/Namioka scanning monochromators for energies below 100 eV and grazing incidence Rowland circle monochromators are used for higher energies

The proceedings of two conferences held at Strathclyde, Scotland, in September of 1967 and 1971, edited by D. J. Fabian and Fabiand and Watson, effectively summarized the state of the theoretical and experimental investigations in the late 1960s. The interpretation of light element spectra in terms of densities of states derived from one electron band structure calculations was well developed, and some many-body effects such as plasmon satellites and spectator holes in d-band metals were understood up to some extent.

It is well known that a typical SXES suffers from low fluorescent yield, small solid angle acceptances at high resolutions, overlapping of orders, low diffraction efficiencies and low detection efficiencies. Therefore, the goal of the soft X-ray emission experimental studies was to overcome these difficulties to have good statistics for the experimental results. Recently, late the development of Synchrotron radiation sources (very low fluorescence yield for soft x-ray is no longer an obstacle for soft x-ray emission spectroscopy) and utilization of spectrometers operated in grazing incidence mode increased the interest of performing these experiments. Typical grazing incidence instruments used for SXES in 1980's by different groups at the Stanford Synchrotron Radiation Laboratory (SSRL) [Rehn et.al., 1974] in Stanford, the National Synchrotron Light Source (NSLS) [William, 1980] in Brookhaven, the Synchrotron Radiation Centre (SRC) [William, 1992] at University of Wisconsin in Madison, the Hamburger Synchrotron Strahlungslabor (HASY) [Saile, 1978] in Humburg , the Berliner Elektronen speicherring- Gesellschaffif Synchrotron Strahlung (BESSY) [Seya, 1952; Namioka, 1954; Greiner and Schaffer, 1957] in Berlin and at the Photon Factory in Tsukuba [Williams, 1992] indicate the increased activity in the field of SXES.

With the explosion of the number of facilities starting in 1980's, most of the attention as far as new designs of the spectrometers, was paid to the energy region of 30 eV to 1 keV. There are three types of monochromators designed and built in most of these facilities. The first type is toroidal/spherical grating monochromator (TGM/SGM) [Himpsel et.al., 1984 ; Dietz et.al., 1985 ; Klaffky, 1982], the second type is Rowland circle monochromator (RCM) [Brown, Stott, and Hulbert, 1986]and the last type is plane-grating monochromator (PGM) [Howells, 1980; Petersen, 1982].

Plane-grating monochromator (PGM) have inherent simplicity. Only a simple rotation of the grating is required for wavelength scanning, so it is comparatively easy to make a UHV compatible monochromator. Usually the small vertical divergence of the source is exploited and the incoming light is considered parallel. In order to obtain a fixed exit beam, it is necessary to use additional mirrors with the plane grating, and the angle of the incidence at the grating and mirror can be chosen to suppress higher orders over a limited wavelength range. Plane grating monochromator dose not have the entrance slit , and it will provide good performance over wide wavelength range

with very low higher order contributions. A variety of good plane gratings are readily available and significant improvements have been made in the fabrication techniques for the aspherical mirrors.

The larger angles of incidence and diffraction of Toroidal grating monochromator (TGM) means that the monochromator can operate at higher energies, but also implies that the aberration are greatly increased. The primary astigmatism of concave grating used at a large angle of incidence is corrected by the toroidal substrated. The defocussing can be minimized by optimizing the entrance and exit arm length for particular wavelength region. Nonlinear rulings with variable grating spacing can be used to correct higher order aberrations. The high energy limit of a TGM is determined primarily by the angular deviation. For operation at high energies the deviation angle must be increased, otherwise the radiation would be absorbed in the grating surface. In order to obtain good resolution, it is necessary to employ a high-frequency grating which increases the dispersion but restricts the spectral range correspondingly. Since a toroidal grating combines both focussing and dispersive properties in a single optical element, for fixed conjugates, it is only possible to optimize the performance over a restricted energy range. Fortunately, most grazing incidence monochromators have a small angular acceptance which means that the aberrations remain tolerably small over an acceptably wide energy range.

The developments in the design of TGM have taken place and become very popular, because of the high photon flux obtained and because of their ease of operation and adequate resolution. Most of the problems are caused by the toroidal gratings. It is difficult to measure the radii of a torus accurately and is even more difficult to polish a toric surface to a particular radius. Fortunately, the approximate focussing of a TGM means that variations in the radii of the torus can be accommodated by varying the arm lengths of the monochromator. The grating has also to be designed for a particular wavelength region, so it is advisable to optimize the mechanical components of the monochromator for the grating rather than vice versa. Since a toroidal grating combines focussing and dispersive properties in a single optical element, it is much more difficult to produce than a conventional grating. As a consequence, there are very few suppliers of high quality toroidal gratings and the prices are rather high particularly for ion-etched gratings

High resolution spectroscopy in the grazing incidence region has been traditionally performed with instruments using the Rowland circle mounting. Although the Rowland mounting provides excellent resolution in its conventional form, it has a disadvantage that the exit beam changes direction as the wavelength is changed. This problem was overcome by using rotating mirror-slit combinations to change the direction of the incoming and outgoing photon [Codling and Mitchell, 1970]. To scan the photon energy range the entrance and the exit slit were fixed as the grating move along the Rowland circle, thus the angular deviation was constant. In the other way, the entrance slit and the grating are fixed and the exit slit will move along the Rowland circle so the angular deviation will change. To obtain high reflectivity at short wavelengths it is necessary to used large angles of incidence. If the angle of incidence decrease as the wavelength is increased, the variation of reflectivity will help suppress higher orders. In this instrument, the angle of incidence increased as the wavelength increased and this combined with the blazed effect tend to limit the usable wavelength range. However the astigmatism of the concave grating at grazing incidence can cause a large loss in intensity.

The best system of the monochromator can only be chosen after considering the characteristics of the source and type of experiments to be performed. If the distance from tangent point to monochromator is large, then plane grating monochromator is the obvious choice. If very high resolution is required, the Rowland circle design should be used. For medium resolution and mechanical simplicity the toroidal grating monochromator represents the optimum. The useful qualities of the Rowland circle monochromators have firmly established them for atomic and molecular physics applications.

Therefore, to overcome the difficulties, people have used monochromators with moving exit slits and detectors, moving entrance slits, multiple gratings for enhancing the operating range, etc, in each of PGM, TGM, and RCM. However an innovative compact, small, flexible spectrometer to cover a long wavelength range of 40 – 1000eV is required for soft X-ray emission spectroscopy experiment (SXES).

At present, there is only one existing commercial high resolution soft X-ray emission spectrometer, supplied by Gammadata (Sweden). The system has been developed by the research group led by Prof. J. Nordgren in Uppsala University,

Uppasala, Sweden [Nordgren, et.al.,1989]. It is based on three interchangeable gratings, which are mounted together with the entrance slit on a slab. These types of gratings are spherical with 5, 5 and 3 m radii, and have a groove densities of 1200, 400 and 300 l/mm, respectively. This spectrometer can cover energy range of ~ 70 - 800 eV in the first order. The grating are blazed to entrance the diffraction efficiency for specific energy (e.g. 275 eV for carbon, 400 eV for nitrogen, and 500 eV for oxygen.). The slit is positioned along the direction of the incoming soft x-ray on the Rowland circles (a circle with half the grating radius on which the slit image is focused) of all three gratings with a grazing angle to the grating of 1.9°, 2.6° and 5.4°, respectively. The schematic of this spectrometer is shown in figure 1.3.

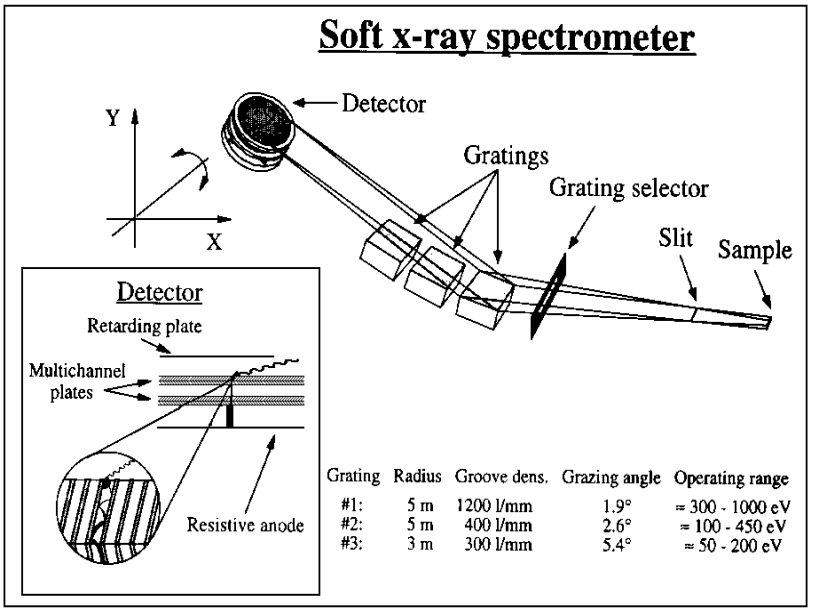

Figure 1.1: *An overview of the soft x-ray emission spectrometer* [Wiell,1995]

In this spectrometer, an entrance slit is used to define the resolving power of the monochromator. A movable multichannel plate (MCP) is used as a detector for mesuring the intensity of the emission.

1.3. Motivation and Purpose

The motivation and purpose of the study is to design a high-resolution soft X-ray spectrometer with comparable or better performance than the existing commercial spectrometer. The optical design obtained will be employed in the spectrometer planned to be attached to the experimental station at Siam Photon laboratory.

Chapter II

Theory

In this chapter, we shall describe the important principles, formulae, and theory used for the evaluation of the soft X-ray spectrometer. The following subsections will give a description of them.

2.1. Grating Equation

Before going further we shall discuss the most important equation describing a grating i.e. grating equation. The equation for a reflection grating is given as:

$$Nk\lambda = \sin\alpha + \sin\beta \qquad 2.1$$

Where

N - groove density

k - order of diffraction

λ- Wavelength

α- Incidence angle

β- Diffraction angle

It can be seen from equation 2.1 [Samson, 1967] that photons with higher energy (lower wavelength) will be diffracted at lower diffraction angle β and vice versa.

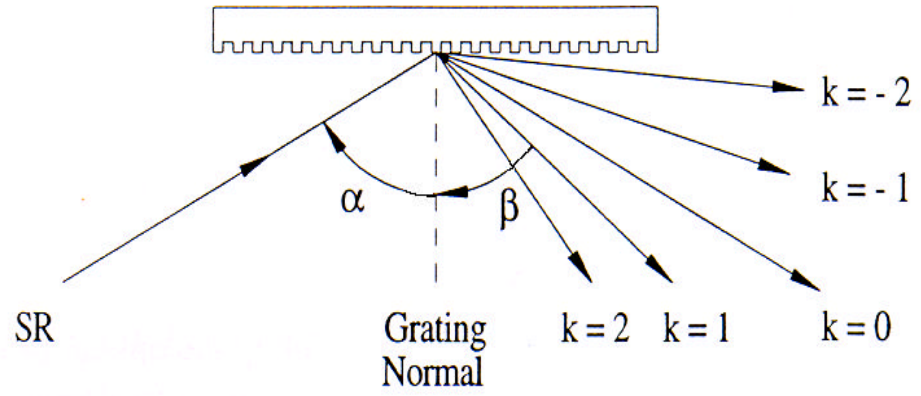

Figure 2.1: *Order of diffraction on diffraction grating* [Peatman, 1997]

The resolution of a spectrometer or a monochromator is decided by the entrance slit, the groove density, the grating radius, and the order of diffraction. It is directly proportional to the diffraction order, e.g. the second order has twice the resolution than in the first order. However, the intensity of the higher light order is generally lower than the lower order. Thus in general, the spectrometers/ monochromators in soft X-ray range are operated only in first or second order. The optical convention followed is that inside orders are obtained by rotating the grating (looking down as shown in figure 2.1) in the clock-wise sense are the positive orders and in the counter clock-wise sense are the negative orders (European Convention).

2.2. Reflectivity

The reflecting property of an optical surface plays a very import role in the evaluation of the efficiency of reflection for a mirror and diffraction efficiency for a grating. The reflectivity of the light incident on an optical surface also depends on the polarization of light. Thus the reflectivity of the light whose electric field vector $(\vec{E})$ perpendicular to the plane of incidence (R_S) and the light with electric field vector $(\vec{E})$ parallel to the plane of incidence (R_P) can be different. The reflectivity can be calculated using the generalized Fresnel equations for reflection [Samson, 1967; Hunter, 1985]:

$$R_s = \frac{(a - \cos\theta)^2 + b^2}{(a + \cos\theta)^2 + b^2} \qquad 2.2$$

$$R_p = R_s \frac{(a - \sin\theta \tan\theta)^2 + b^2}{(a + \sin\theta \tan\theta)^2 + b^2} \qquad 2.3$$

Where θ is the angle of incidence with respect to the surface normal.

$$a^2 = \frac{1}{2}\left\{\left[(n^2 - k^2 - \sin^2\theta)^2 + 4n^2k^2\right]^{1/2} + (n^2 - k^2 - \sin^2\theta)\right\} \qquad 2.4$$

$$b^2 = \frac{1}{2}\left\{\left[(n^2 - k^2 - \sin^2\theta)^2 + 4n^2k^2\right]^{1/2} - (n^2 - k^2 - \sin^2\theta)\right\} \qquad 2.5$$

Hence, if one knows the optical constants (n and k) of a material at some photon energy wavelength or energy, one can calculate the components of reflectivity at that energy for any angle of incidence, θ.The complex index of reflection, n(E) , is defined in term of the optical constants n and k:

$$\tilde{n}(E) = n(E) + ik(E) \qquad 2.6$$

where n(E) is the real part and the usual index of refraction
and k(E) is the imaginary part and extinction coefficient.

The fundamental reflection properties devide the monochromator/spectrometer design into two areas namely grazing and normal incidence instruments. The grazing incidence angle instruments typically cover the range from 20 eV upward to many thousands of electron volts where as the normal incidence instruments cover the energy range 1 – 40 eV. Normal incidence geometry is more desirable than grazing incidence because of the reduced problems with astigmatism and other aberrations and is the geometry of choice wherever possible. In the photon energy region above 100 eV, reflection efficiencies above 90% can readily be achieved at grazing angles of around 0.5° (10 mrad) [Henke, et.al., 1982]. Figure 2.2 shows the variation of reflectivity of gold for various angle of incidence and cover the photon energy range 100-2000 eV. This figure indicates the importance of angle of incidence for obtaining better reflectivities at a given photon energy.

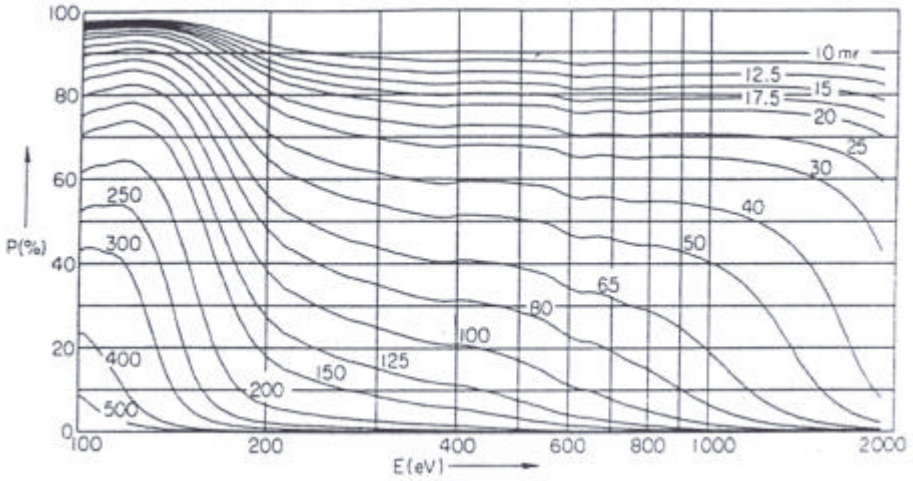

Figure 2.2: *Variation of percentage reflectivity for gold from 100 eV to 2000 eV at various grazing incidence angles give in mrad* [Williams. 1992]

2.3. Grating Efficiency

Grating efficiency depends on the shape and of nature of the groove of a grating. In the soft x-ray energy range of interest, blazed gratings are found to offer best efficiency in the first order. The efficiency of a blazed grating depends upon the blaze angle and blaze wavelength. The details of the blazed grating parameters and the dependence of the efficiency on the blaze parameters are described as follows. A blazed grating is shown in Figure 2.3. In the figure, N is the normal to the overall grating surface while N′ is the normal to the individual facet. The grating considered is in a constant ruling density type.

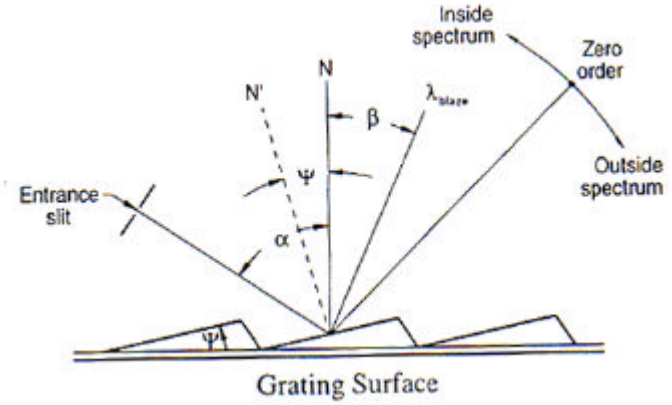

Figure 2.3: *The blaze angle of a diffraction grating* [Peatman, 1997]

For the blazed grating, it is possible to have a diffraction condition such that the diffracted beam is specularly reflected from the angled grooves. This situation is given by:

$$a - \Psi = -b + \Psi \qquad 2.7$$

$$\Psi = \frac{a + b}{2} \qquad 2.8$$

Where α is incidence angle

β is diffraction angle

ψ is blaze angle

The sign convention of α and β are of opposite sign when they are on the opposite sides of the normal. Half of the deviation angle of the grating is

$$q = \frac{a - b}{2} \qquad 2.9$$

Using the grating equation 2.1 and equation 2.9 we can obtain

$$l = \frac{2}{Nk} \cos q \sin \Psi \qquad 2.10$$

Therefore

$$l_{blaze} = \frac{2}{Nk} \cos (a - \Psi) \sin \Psi \qquad 2.11$$

Where θ is deviation angle

N is groove density

k is order of diffraction

λ_{blaze} is the wavelength at the blaze angle

From this equation, without including other effects, we know that a grating blazed for the wavelength λ in the first order (k=1) is blazed for λ/2 in second order (k=2) etc..

The reflection efficiency of coating is a function of the coating material of the grating surface, its roughness, its thickness, the angle of incidence and the wavelength of the photon to be reflected. Basically, the thickness of the coating must be sufficient so that no interference occurs between the top and the bottom of the coating layer, where a change in the indices of reflection occurs at each interface. Vice versa, the extinction lengths of the photon wavelengths used must be shorter than the optical path in the coating so that the photon does not reach the second interface. The thickness of the coatings are between 400 and 600 Å [Peatman, 1997]. The most commonly used coatings material in the grazing incidence region are gold, platinum, and rhodium because of their reflectivity and because they can be evaporated onto the substrate with very small micro-roughness of the order of few angstrom. In the region of soft x-rays, gold is the best material for coatings.

2.4 Fermat's Principle.

Fermat's principle plays an important role in describing the geometric theory of the diffraction grating. Fermat's principle states that

"*when a light ray travels between any two points A and B, it's actual path will be the one that requires the least time*" [Born and Wolf, 1980; Jenkins and White, 1976].

To illustrate the Fermat's principle we shall use the case of a ray incident on the surface of a grating as shown in Figure 2.5. When the refraction index of the grating is a constant, light ray starting at point A and travels in a straight line impinging on a grating at point $P_{\xi, \omega, L}$ and then reflect to point B in space. The same is shown in Figure 2.4. According to Fermat's Principle, if point A is to be imaged at

some point B, then all of the paths from A via the surface of grating, described by $P_{\xi, \omega, L}$ to B must be equally long. In other words, the times taken by light rays in going from one point to the other must be the same.

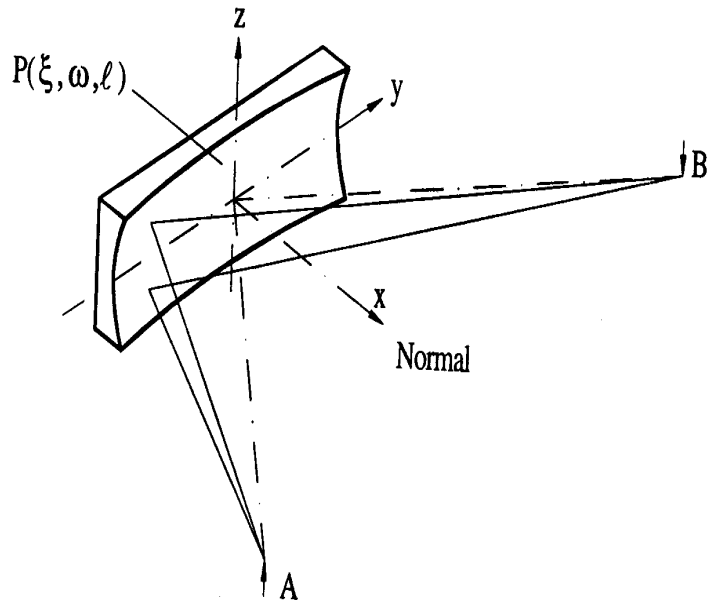

Figure 2.4: *The coordination system for optical path function* [Peatman, 1997]

Thus, it is the job of the grating to accomplish this. If the grating is in the correct geometry, the image will be ideal and otherwise no image or a poor image will be the result. This will happen continuously over the possible paths if the paths are equally long.

2.5. Theory of Diffraction Grating:

Fermat's principle explains the behavior of optical systems. In case of diffraction grating, the phase advance of the radiation that occurs at the grating must be included in the optical path function as " $Nk\lambda\omega$ ". If the light is coming from point

A and impinging on an arbitrary point P (ξ,ω, ℓ) of the diffraction grating, and then contribute the image at point B (see Figure 2.5).

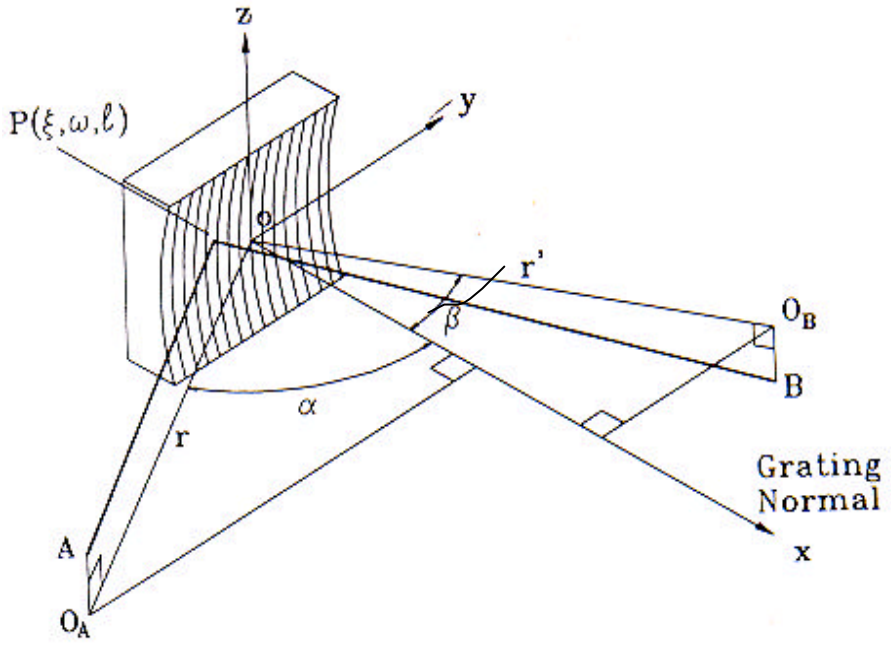

Figure 2.5: *Theory of diffraction grating* [Peatman, 1997]

The optical path, F, is

$$F = \overline{AP} + \overline{PB} + Nk\,\boldsymbol{l}\boldsymbol{w} \qquad 2.12$$

Where N is the line density

k is the order of diffraction ±1, ±2, etc.

λ is the wavelength of the ligth being diffracted

ω is the position in the dispersion plane.

If the Fermat's principle is fulfilled, rays of light coming from A will be arrive at B with the same phase. The conditions for focussing A at B are given by

$$\frac{\P F}{\P \boldsymbol{w}} = 0 \qquad \textit{and} \qquad \frac{\P F}{\P \ell} = 0 \qquad 2.13$$

A point in the image plane where is a derivative of the path function with respect to ω equal zero, is called "a meridional focus". This is in the dispersion plane of the grating and is the critical one for energy resolution. In another case, where the derivative of the path function with respect to ℓ equal zero is called "sagittal focus". If these two foci do not coincide then the system is said to be astigmatic.

Equations 2.12 and 2.13 forms the basis for determining the optical properties of a diffraction grating. We can use these equations in designing the characteristics of the required diffraction grating, such as, the shape of the surface and the groove density (N) in order to optimize the performance of the system. The primary focussing and the reduction of aberrations can be obtained by the suitable variation of the groove density of the grating. If we consider constant spacing diffraction gratings, we should develop the relationship between the geometry of the optical system and the dispersion resulting from this geometry, the aberration dispersion.

It is convenient to use a polynomial representation for the surface P (ξ, ω, ℓ) = 0,

Where $$x = \sum_{i=0}^{\infty}\sum_{j=0}^{\infty} a_{ij} w^i \ell^j \qquad 2.14$$

and $a_{00} = a_{10} = 0$ and j is even

We examine the surface at the origin of the xy plane. By using the coefficients given in the table 2.1 for the spherical surface illustrated in Figure 2.5.,we obtain,

$$\vec{AP} = A\vec{O}_A + \vec{O_A A} + \vec{OP} = \begin{pmatrix} 0 \\ 0 \\ -z \end{pmatrix} + \begin{pmatrix} -r\cos\alpha \\ -r\sin\alpha \\ 0 \end{pmatrix} + \begin{pmatrix} x \\ w \\ \ell \end{pmatrix} \qquad 2.15$$

$$\overline{AP} = \left|\vec{AP}\right| = \left[(x - r\cos\alpha)^2 + (w - r\sin\alpha)^2 + (\ell - z)^2\right]^{\frac{1}{2}} \qquad 2.16$$

$$\overline{BP} = \left|\vec{AP}\right| = \left[(x - r'\cos\alpha)^2 + (w - r'\sin\alpha)^2 + (\ell - z')^2\right]^{\frac{1}{2}} \qquad 2.17$$

For the central ray $\left(\frac{\partial F}{\partial \ell}\right)_{x=w=\ell=0} = 0$ Leading to $\frac{z}{r} = -\frac{z'}{r'}$

Table 2.1: The a_{ij} coefficients at the optical path function for spherical surfaces

$a_{02} = \frac{1}{2r}$	$a_{20} = \frac{1}{2R}$	$a_{22} = \frac{1}{4R^2 r}$	
$a_{40} = \frac{1}{8R^3}$	$a_{04} = \frac{1}{8r^3}$	$a_{12} = 0$	$a_{30} = 0$

If points A and B lie on opposites sides of the grating normal, the signs of α and β are opposite . The grating dimensions are $\pm\omega_0$ in the y direction and $\pm\ell_0$ in the sagittal direction. The origin is at the center of the grating. From the geometric relations relating A, P and B, the variables x, y, x', y', and from the expression of ξ in term of a_{ij} (that given in table 2.1), we can express F as follows;

$$F = F_{000} + wF_{100} + \frac{1}{2}w^2 F_{200} + \frac{1}{2}\ell^2 F_{020} + \frac{1}{2}w^3 F_{300} + \frac{1}{2}w\ell^2 F_{120} + \frac{1}{8}w^4 F_{400}$$
$$+ \frac{1}{4}w^2\ell^2 F_{220} + \frac{1}{8}\ell^4 F_{040} + \ell F_{011} + w\ell F_{111} + \frac{1}{2}wF_{102} + \frac{1}{4}w^2 F_{202} + \frac{1}{2}w^2 \ell F_{211} + \ldots$$

We can expand each important term, and it can tell us about the optical properties of the grating surface. Using the notation of Noda et al. [Noda, Namioka, Seya, 1974], each term of F will be shown as follows:

$F_{000} = r + r'$ optical path

$F_{100} = Nk\lambda - (\sin\alpha + \sin\beta)$ grating equation

$F_{200} = \left(\frac{\cos^2\alpha}{r}\right) + \left(\frac{\cos^2\beta}{r'}\right) - 2a_{20}(\cos\alpha + \cos\beta)$ meridional focus

$$F_{020} = \frac{1}{r} + \frac{1}{r'} - 2a_{02}(\cos\alpha + \cos\beta)$$ sagital focus

$$F_{120} = \left[\frac{S(r,\alpha)}{r}\right]\sin\alpha + \left[\frac{S(r',\beta)}{r'}\right]\sin\beta - 2a_{12}(\cos\alpha + \cos\beta)$$ astigmatic coma

$$F_{300} = \left[\frac{T(r,\alpha)}{r}\right]\sin\alpha + \left[\frac{T(r',\beta)}{r'}\right]\sin\beta - 2a_{30}(\cos\alpha + \cos\beta)$$ primary coma

$$F_{400} = \left[\frac{4T(r,\alpha)}{r^2}\right]\sin^2\alpha - \left[\frac{T^2(r,\alpha)}{r}\right] + \left[\frac{4T(r',\beta)}{r'^2}\right]\sin^2\beta - \left[\frac{T^2(r',\beta)}{r'}\right]$$
$$- 8a_{30}\left[\frac{1}{r}(\sin\alpha\cos\alpha) + \frac{1}{r'}(\sin\beta\cos\beta)\right] - 8a_{40}(\cos\alpha + \cos\beta) + 4a_{20}^2\left[\frac{1}{r} + \frac{1}{r'}\right]$$

$$F_{220} = \left[\frac{2S(r,\alpha)}{r^2}\right]\sin^2\alpha + \left[\frac{2S(r',\beta)}{r'^2}\right]\sin^2\beta - \left[\frac{T(r,\alpha)S(r,\alpha)}{r}\right] - \left[\frac{T(r',\beta)S(r',\beta)}{r'}\right]$$
$$+ 4a_{20}a_{02}\left[\frac{1}{r} + \frac{1}{r'}\right] - 4a_{22}(\cos\alpha + \cos\beta) - 4a_{12}\left[\frac{1}{r}(\sin\alpha\cos\alpha) + \frac{1}{r'}(\sin\beta\cos\beta)\right]$$

$$F_{040} = 4a_{02}^2\left[\frac{1}{r} + \frac{1}{r'}\right] - 8a_{04}(\cos\alpha + \cos\beta) - \left[\frac{S^2(r,\alpha)}{r}\right] - \left[\frac{S^2(r',\beta)}{r'}\right]$$

$$F_{011} = \frac{-z}{r} + \frac{-z'}{r'}$$

$$F_{111} = -\frac{z\sin\alpha}{r^2} - \frac{z'\sin\beta}{r'^2}$$

$$F_{102} = \frac{z\sin\alpha}{r^2} - \frac{z'\sin\beta}{r'^2}$$

$$F_{202} = \left(\frac{z}{r}\right)^2\left[\frac{2\sin^2\alpha}{r} - T(r,\alpha)\right] + \left(\frac{z'}{r'}\right)^2\left[\frac{2\sin^2\beta}{r'} - T(r',\beta)\right]$$

$$F_{211} = \frac{z}{r^2}\left[T(r,\alpha) - \frac{2\sin^2\alpha}{r}\right] + \frac{z'}{r'^2}\left[T(r',\beta) - \frac{2\sin^2\beta}{r'}\right]$$

where $T(r,\alpha) = \left(\frac{\cos^2\alpha}{r}\right) - 2a_{20}\cos\alpha$ and $S(r,\alpha) = \frac{1}{r} - 2a_{02}\cos\alpha$

$T(r', \beta)$ and $S(r', \beta)$ can be find in the same way with these.

The aim of this work is not only determine the relationship between A, P and B, but also find the resolution, $\Delta\lambda$, of the grating. To achieve these objectives, let us separate the optical path function F into two terms as

$F^{*} = F_{000} + \omega F_{100}$ and F^{**} = the rest F_{ijk} terms of the optical path function

Application of the Fermat's principle will help in deriving the expression for $\Delta\lambda$ as follows:

start with the grating equation $$Nk\lambda = \sin\alpha + \sin\beta$$

differentiate this equation with β $$\left(\frac{\partial \lambda}{\partial \beta}\right)_{\alpha = const.} = \frac{1}{Nk}\cos\beta$$

since $\frac{dy'}{r'} = d\beta$, we get $$d\lambda = \frac{1}{Nk}\frac{\cos\beta}{r'}dy'$$

Thus the deviation of the path function in the dispersive direction is

$$\frac{\partial F^{**}}{\partial \omega} = d(\cos\gamma_y) = d(\sin\beta) = \cos\beta\, d\beta = \frac{\cos\beta}{r'}dy'$$

where δ (cos γ_y) is the change in direction cosine from the Gaussian value [Howells, 1980] and the deviation in the sagittal direction is given by:

$$\frac{\partial F^{**}}{\partial \ell} = \frac{1}{r'}dz'$$

Therefore $$\Delta\lambda = \frac{1}{Nk}\cdot\frac{\partial F^{**}}{\partial \omega}$$

The final expression for resolution is

$$\Delta\lambda = \frac{1}{Nk}\left[\omega F_{200} + \frac{3}{2}\omega^2 F_{300} + \frac{1}{2}\ell^2 F_{120} + \frac{1}{2}\omega^3 F_{400} + \frac{1}{2}\omega\ell^2 F_{220} + \ell F_{111} + \frac{1}{2}F_{102} + \frac{1}{2}\omega F_{202} + \omega\ell F_{211} + \ldots\right] \qquad 2.18$$

From the above expressions it is easy to understand the importance of each term of the optical path function, grating equation, sagittal and meridinal focus, and coma and their mutual dependence. The next step is to summarize the grating theory in the interested cases of surfaces i.e. toroidal and spherical by using the optical path function. For spherical grating, by expanding the optical path function, the individual evaluation of different parameters and aberrations can be obtained. They are:

$$F_{100} = Nk\,l - (\sin\alpha + \sin\beta)$$ grating equation

$$F_{200} = \left(\frac{\cos^2\alpha}{r} - \frac{\cos\alpha}{R}\right) + \left(\frac{\cos^2\beta}{r'} - \frac{\cos\beta}{R}\right)$$ meridional focus

$$F_{020} = \frac{1}{r} + \frac{1}{r'} - \frac{1}{\rho}(\cos\alpha + \cos\beta)$$ sagital focus

$$F_{300} = \left[\frac{\cos^2\alpha}{r} - \frac{\cos\alpha}{R}\right]\frac{\sin\alpha}{r} + \left[\frac{\cos^2\beta}{r'} - \frac{\cos\beta}{R}\right]\frac{\sin\beta}{r'}$$ primary coma

$$F_{120} = \left[\frac{1}{r} + \frac{\cos\alpha}{\rho}\right]\frac{\sin\alpha}{r} + \left[\frac{1}{r'} + \frac{\cos\beta}{\rho}\right]\frac{\sin\beta}{r'}$$ astigmatic coma

$$F_{400} = \frac{4}{r^2}\left[\frac{\cos^2\alpha}{r} - \frac{\cos\alpha}{R}\right]\sin^2\alpha - \frac{1}{r}\left[\frac{\cos^2\alpha}{r} - \frac{\cos\alpha}{R}\right]^2 + \frac{4}{r'^2}\left[\frac{\cos^2\beta}{r'} - \frac{\cos\beta}{R}\right]\sin^2\beta$$
$$- \frac{1}{r'}\left[\frac{\cos^2\beta}{r'} - \frac{\cos\beta}{R}\right]^2 - \frac{1}{R^3}(\cos\alpha + \cos\beta) + \frac{1}{R^2}\left[\frac{1}{r} + \frac{1}{r'}\right]$$

$$F_{202} = \left(\frac{z}{r}\right)^2\left[\frac{2\sin^2\alpha}{r} - \frac{\cos^2\alpha}{r} + \frac{\cos\alpha}{R}\right] + \left(\frac{z'}{r'}\right)^2\left[\frac{2\sin^2\beta}{r'} - \frac{\cos^2\beta}{r'} + \frac{\cos\beta}{R}\right]$$

$$F_{211} = \frac{z}{r^2}\left[\frac{\cos^2 \alpha}{r} - \frac{\cos \alpha}{R} - \frac{2\sin^2 \alpha}{r}\right] + \frac{z'}{r'^2}\left[\frac{\cos^2 \beta}{r'} - \frac{\cos \beta}{R} - \frac{2\sin^2 \beta}{r'}\right]$$

$$F_{220} = \left[\frac{1}{r} - \frac{\cos \alpha}{r}\right]\frac{2\sin^2 \alpha}{r^2} + \left[\frac{1}{r'} - \frac{\cos \beta}{r}\right]\frac{2\sin^2 \beta}{r'^2} - \frac{1}{r}\left[\frac{\cos^2 \alpha}{r} - \frac{\cos \alpha}{R}\right]\left[\frac{1}{r} - \frac{\cos \alpha}{r}\right]$$
$$- \frac{1}{r'}\left[\frac{\cos^2 \beta}{r'} - \frac{\cos \beta}{R}\right]\left[\frac{1}{r'} - \frac{\cos \beta}{r}\right] + \frac{1}{rR}\left[\frac{1}{r} + \frac{1}{r'}\right] - \frac{1}{rR^2}(\cos \alpha + \cos \beta)$$

$$F_{011} = \frac{-z}{r} + \frac{-z'}{r'}$$

$$F_{111} = -\frac{z\sin \alpha}{r^2} - \frac{z'\sin \beta}{r'^2}$$

$$F_{102} = \frac{z\sin \alpha}{r^2} - \frac{z'\sin \beta}{r'^2}$$

The resolution is related to the various terms of the optical path function. It is given by the following:

$$\Delta l = \frac{1}{Nk}\left[w F_{200} + \frac{3}{2}w^2 F_{300} + \frac{1}{2}\ell^2 F_{120} + \frac{1}{2}w^3 F_{400} + \frac{1}{2}w\ell^2 F_{220} + \ell F_{111}\right.$$
$$\left. + \frac{1}{2}F_{102} + \frac{1}{2}wF_{202} + w\ell F_{211} + \ldots\right]$$

To obtain the best resolution, the most important thing to do is to minimize F_{200} term. But it cannot be done for all wavelengths. Since the monochromators/ spectrometers are designed for more than one user group and for more than one type of experiment and covering a large energy range, obtaining good energy resolution will be beyond the ability of one grating. The number of gratings to be used in a spectrometer depend on the operating range, the overlap of energy ranges of the gratings, shape of the grating and the design geometry.

In a plane grating monochromator/spectrometer we require only one or two grating to cover the large energy range. For an experiment with a requirement of long and continuous energy scan and for a plane grating monochromator/spectrometer there is no need to change a grating. The profile of the plane grating can be blaze or laminar. Line densities of between 300 and 1200 lines/mm for a plane can cover the energy range between 10 eV and 200 eV [Peatman, 1997].

For spherical/toroidal grating monochromaters/spectrometer the allowed turning range of the grating is based on the condition that the grating must focus the entrance slit on the exit slit. Obtaining this is possible only with a change in entrance or exit arm lengths. For a given deviation angle geometry, arm lengths and energy range is determined by the groove density of the grating. An increase in the groove density will increase the dispersion and the energy range. However to have sufficient efficiency over a large energy range several gratings are used in there monochromators/spectrometers.

To decide the choice of grating to be used in a spectrometer the basic considerations are the following:

- Energy range
- Resolution required
- Flux required
- The grating type
- The number of grating to be used for the energy range desired
- Availability of the type of grating desired
- Cost of the grating
- Space available for the spectrometer
- Complexity and cost of the mechanics
- Amount of manpower required to use and maintain the spectrometer.

To address some of these points, knowledge of grating theory mentioned will play a significant role. For confirmation, a detailed set of analytical calculations and exact ray tracing will be essential. It is equally important to have knowledge of the experiments for which the spectrometer is to be designed. Thus, the end users play an important role in the choice of spectrometer.

2.6 The Rowland Circle Geometry

This geometry offers better resolution than the toriodal/spherical grating instruments in constant deviation mount. This was originally proposed by H.A. Rowland for the minimizing the aberrations of a grating [Rowland, 1882 and 1883]. A classical Rowland circle monochromator is shown in Figure 2.6. The grating radius is equal to the diameter of the circle, while the Rowland circle gives the position of both slits. Our plan of spectrometer designs is based on this basic geometry. This geometry is used and explained at length in this thesis.

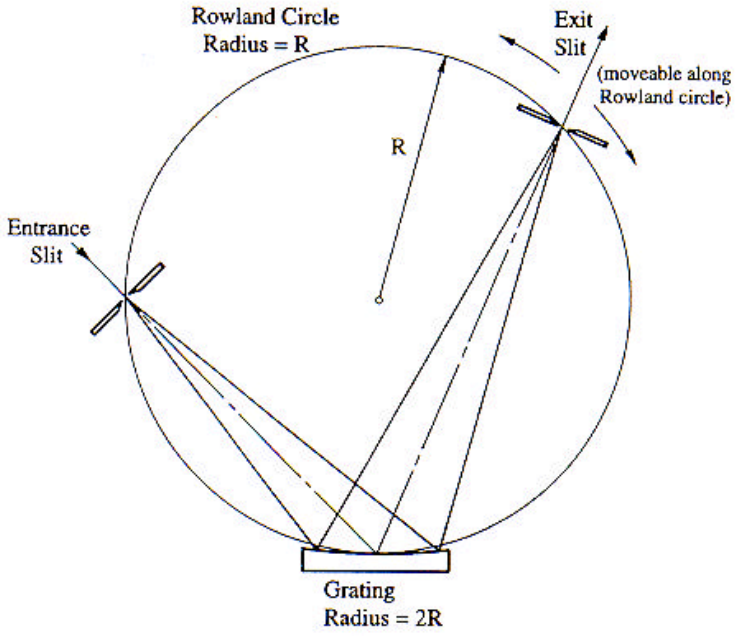

Figure 2.6: *The layout of a classical Rowland circle monochromator* [Peatman, 1997]

Rowland circle geometry for the grazing incidence region of the spectrum has been used to built monochromators at many Synchrotron Radiation Laboratories [Ishiguro, et.al., 1989; Senf, Eggenstein and Peatman, 1992; Senf, et.al., 1989]. In this geometry grating is rotated according to the grating equation. The Rowland conditions are fulfilled with few optical components at grazing incidence and with a constant overall length of the monochromator.

From the F_{ijk} terms described in the spherical grating case, Rowland identified the following terms which are common to meridional (de) focussing, coma and parts of the spherical aberrations:

$$\left[\frac{\cos^2 \alpha}{r} - \frac{\cos \alpha}{R}\right] \quad \text{and} \quad \left[\frac{\cos^2 b}{r'} - \frac{\cos b}{R}\right]$$

Furthermore, he solved each term independently of other, thereby making a general solution to the aberration equations and gets the solutions they are:

$$r = R\cos\alpha \qquad and \qquad r' = R\cos b$$

These are the Rowland conditions for spherical grating monochromator. If we insert them into the F_{ijk} term, the optical path function of The Rowland circle monochromator are as following:

Grating equation is $$F_{100} = Nk\lambda - (\sin\alpha + \sin b)$$

Sagittal focus is $$F_{020} = \frac{1}{r} + \frac{1}{r'} - \frac{1}{\rho}(\cos\alpha + \cos b)$$

Meridional focus is $$F_{200} \equiv 0$$

Primary coma is $$F_{300} \equiv 0$$

and $$F_{400} = -\frac{1}{R^3}(\cos\alpha + \cos b) + \frac{1}{R^2}\left(\frac{1}{r} + \frac{1}{r'}\right)$$

Thus we get the resolution for this type of monochromator by the equation:

$$\Delta E = \frac{E^2 s'}{CkNR} \qquad 2.19$$

Where E is a photon energy

C is a constant

s′ is the exit slit width

R is the radius of Rowland circle.

From this equation it is clear that resolution decreases with increasing photon energy for this mounting. Therefore, to obtain uniform average high resolution several gratings are required for spherical grating monochromators in this configuration. Because a monochromator consists of the slits and the grating, the resolution is limited by slit widths apart from the grating parameters. We can find the slit width limited resolution equation directly from the grating equation as:

For the entrance slit $$\Delta \lambda_{ent} = \frac{1}{Nk}\frac{s}{r}\cos\alpha \qquad 2.20$$

For the exit slit $$\Delta \lambda_{exit} = \frac{1}{Nk}\frac{s'}{r'}\cos\beta \qquad 2.21$$

Where s is the entrance slit width

and s' is the exit slit width.

The optimal size of the exit slit width for given entrance slit or source size depends upon the magnification of the monochromator, M(λ). The magnification of a monochromator is given by

$$M(\lambda) = \frac{s'}{s} \qquad 2.22$$

Using this equation and substituting in the Rowland condition, the magnification of the Rowland circle monochromator is

$$M(\lambda) = \frac{s'}{s} = \frac{R\cos\beta\cos\alpha}{R\cos\alpha\cos\beta} \equiv 1$$

Thus no demagnification is possible in this geometry and nothing can be done about the source size within a Rowland circle instrument. For such a monochromator the grating length can be found by using this following equation

$$\text{Grating length} \cong \frac{2\,r\,\sin\,m}{\sin\,\theta_g} \qquad 2.23$$

where θ_g is the grazing angle, 2m is the full vertical acceptance and r is the distance between entrance slit and grating. For the Rowland circle geometry the entrance and exit arm length depends on the radius of the grating and are calculated using the following equation:

$$\text{Entrance armlength } (r) = R\cos\alpha \qquad 2.24$$

$$\text{Exit armlength } (r') = R\cos\beta \qquad 2.25$$

where R, α, and β are radius of the spherical grating, angle of incidence and angle of reflection respectively. The displacement of the detector along the Rowland circle can be found by using cosine law , that is

$$a^2 = b^2 + c^2 - 2bc\cos\Delta\beta \qquad 2.26$$

Where a, b, c and $\Delta\beta$ are shown in the Figure 2.7

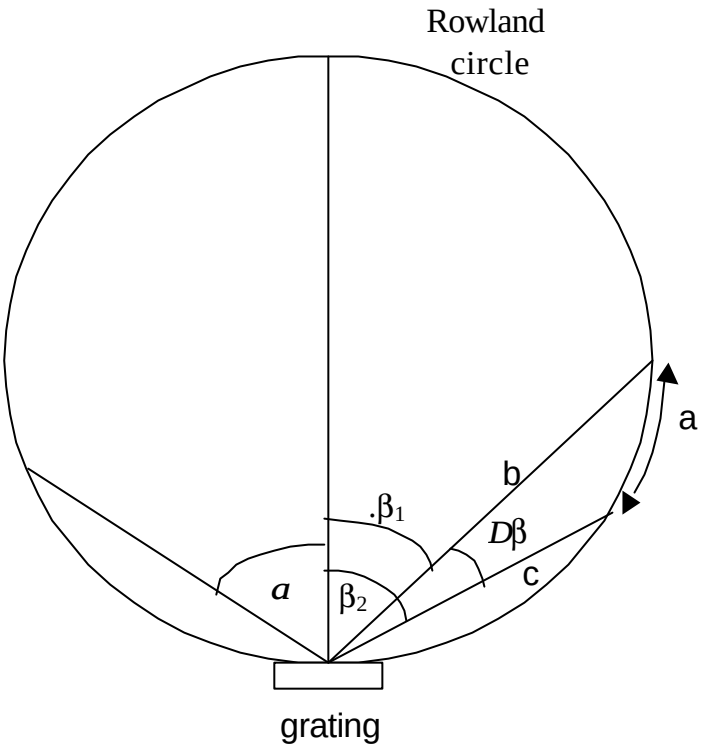

Figure 2.7: *Displacement of the detector on the Rowland circle geomatry*

Where :

a is the displacement on the Rowland circle geometry

b is the exit arm length of the first diffracted photon in the interested energy range

c is the exit arm length of the last diffracted photon in the interested energy range

$\Delta\beta = \beta_2 - \beta_1$ is the difference in diffraction angles for the beginning and end of the energy range of operation

2.7 Detector

The diffracted photons from the sample are detected using a two-dimensional (area) detector. The detector is movable in the normal plane of the gratings and the slit, and rotatable with a rotation axis through the detector center and perpendicular to this plane. The detector is placed tangential to the grating used in Rowland circle.

The detector used in this work is microchannel plate (MCP) where the surface of the first plate is covered by a 3000 Å thick CsI layer [Michette and Buckley, 1993] in order to enhance the electron emission induced by incoming photons. MCP is a secondary electron multiplier consisting of an array of millions of glass capillaries (channels) having an internal diameter ranging from 10μm to 20μm [Adams and Manley, 1966] fused into the from of thin disk less than 1 mm thick (see Figure 2.8). The inside wall of each channel is coated with a secondary electron emissive material having a proper resistance and both ends of the channel are covered with a metal thin film which acts as electrodes, thus each channel becomes an independent secondary electron multiplier.

When a voltage V_D is applied the both sides of an MCP as show in Figure2.9, the electric field is generated in the direction of the channel axis. As an electron hits the entrance wall of the channel, secondary electrons are produced.

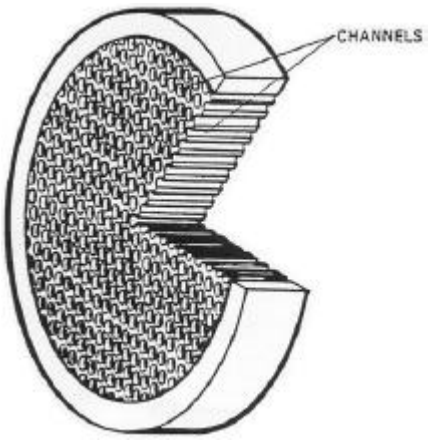

Figure 2.8: *Schematic construction of a MCP* [Michette and Buckley, 1993]

These secondary electrons are accelerated by the electric field, and travel along the parabolic trajectories determined by their initial velocity. Then they strike

the oposite wall and produce secondary electrons further. This process is repeated many times along the channel and as a result the electron current increases exponentia lly towards the output end of the channel.

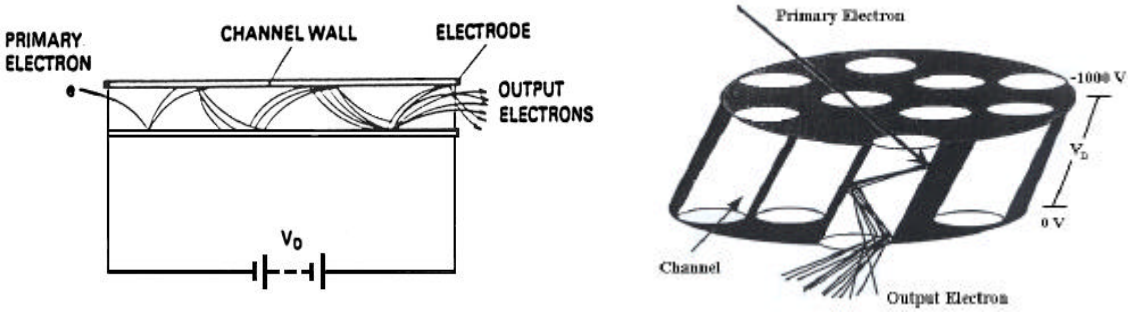

Figure 2.9: *Principle of electron amplification* [Michette and Buckley, 1993]

The multiplication mechanism is shown in Figure 2.9. MCP shows many special features described as follows:

1. High gain
2. Two- dimensional image intensification
3. Fast time response
4. Imunity to magnetic Fields
5. Sensitive to charged particle, UV, and X-rays
6. Low power consumption
7. Small size, light weight
8. Easy to handle because of two terminals
9. Stable in air.

MCP can be used as detectors of X-rays, UV light, charged particles and in observation of images produced by these particles.

Chapter III

Optical Evaluation and Ray Tracing

The first step in designing of a spectrometer is to know the specification of its purpose and the expected performance (wavelength coverage, spectral, resolution, etc.). The next step is to choose the candidate configuration that will meet the goals and to lay them out in the physical space available using first-order i.e. paraxial and geometrical optics theory. This methodology establishes the object and image distances, focal lengths, spectral dispersion, etc. enabling a first order evaluation of the instrument performance to be made. A satisfactory paraxial design establishment paves the way for the detailed performance evaluation of the spectrometer. At this point using higher order geometrical optics theory and exact ray tracing, the possible image defects or aberrations encountered and the effect of these aberrations on the imaging performance of the optical instrument should be analyzed.

3.1 Design Criteria

From Chapter II we provide some information about the optical elements in the spectrometer. In this chapter we will discuss about the design methodology of the spectrometer. There are three steps in the designing of the spectrometer.

STEP-1:

- Operating Energy Range

In soft x-ray emission spectroscopy the energy range of interest is from 50 eV to 1000 eV and the spectrometer should cover this range of energies.

- Resolving Power

Two close wavelengths (λ and $\lambda+\Delta\lambda$) of the same intensity of the diffracted wavelengths can still be distinguished when the maximum of the diffraction pattern of

λ lies at the first minimum of the diffraction pattern of $\lambda+\Delta\lambda$ (Raleigh's criterion). If the two diffraction pattern do not follow this criterion the wavelength difference ($\Delta\lambda$) between two peaks will no longer be resolved correctly. Thus the resolving power R is defined as $\lambda/\Delta\lambda$ where $\Delta\lambda$ is the minimal separation of wavelengths which can be achieved at the wavelength λ.

- Flux Requirement

This is defined by the nature of experiments planned using the instrument considered for design. This parameter is related to the resolution of the spectrometer at which it is going to operate while the experiment is performed. To obtain the high resolving power, the spectrometer should use smaller slit width (entrance slit) which will reduce the flux, and at the same time, by sacrificing the resolution one can obtain better flux.

- Number of Gratings

This will depend on the energy range of operation of the spectrometer i.e. 40 –1000 eV. For spectrometers using spherical grating (this case) only one grating will not give the high efficiency of the diffracted light for the whole energy range. Therefore the number of the gratings to be used should be at least two or three depend on the efficiency of the gratings for the specified energy range.

- Type of The Gratings

Type of the grating that satisfies the requirement in this case is a concave diffraction grating (spherical grating). The utilization of a concave grating greatly simplifies the alignment, operation, focus, apart from low-cost and high efficient spectral system (only one optical element and one mount and single reflection) required to generate a given spectrum. It is to be mentioned here that the geometry of the spherical grating used in the soft X-ray spectrometer will depend on the aims mentioned earlier i.e. high resolution coupled with high flux.

- Entrance Slit

To get the high resolution of the spectra smaller entrance slit width should be used in the spectrometer.

STEP-2:

- The Choice of Deviation Angle, a -b

The choice of the deviation angle to be used in the spectrometer depends on the reflectivities of the grating ($R_s$and R_p). For the grazing incidence instruments i.e. instruments cover the energy range from 20 eV upward to 1000 eV the choice of α, β and the deflection angle, α -β is give by the condition

$$\frac{l_2}{l_1} = \frac{\sin f_2}{\sin f_1} \quad \text{where} \quad f = \frac{a+b}{2}$$

ϕ_1-ϕ_2 is the angular scanning rage of the grating for the wavelength range λ_1-λ_2 .

If a variable α -β is to be used, it should increase with increasing photon energy for high order light suppression.

- Size of The Spectrometer:

This is determined by the total space available, the space required for the experiments, etc. The size of the spectrometer depends on the grating length, grating radius, the entrance and exit arm length, the number of optical elements to be used, and the space required for alignment of the optical elements in the spectrometer.

- Minimization of Optical Aberrations

Different terms in the optical path function represent a particular type of aberration. The minimization all these aberration terms is important for obtaining the best performance from the spectrometer. For example, Rowland identified the following terms which are common to meridional focussing, coma and parts of the spherical aberrations.

STEP-3:

The availability of the optical components desired and the means of suppression of higher orders

3.2 Ray Tracing Program

By using the design considerations, the model of the spectrometer and the layout is obtained. The next step is to optimize the configuration of the spectrometer. This can be achieved by performing exact ray-tracing with the help of a ray tracing programs. The three basic optical principles used in a ray tracing program are:

1. The optical path between physical elements of the optical system is along a straight line.
2. The angle of reflection is equal to the angle of incidence.
3. Bragg's law governs the diffraction phenomena.

There are many ray-tracing programs available commercially and some can be obtained freely for research purposes. One of such programs called "RAY" (version number 24.1). was obtained from BESSY, Berlin, Germany, for performing this evaluation. The development of "RAY" at BESSY is in progress from 1984 for ray-tracing evaluation of VUV and soft x-ray optical schemes [Schäfers, 1996]. This program simulates the source of our choice and evaluates the imaging and focussing properties of an optical system by means of exact ray tracing. Various interesting features like focal properties, power distribution, energy resolution, rocking curves, absolute transmission and polarization characteristics of an optical setup can be simulated using this program. The coordinates system used in "Ray" program is shown in the figure 3.1. The coordinate system is transformed along the optical path from the source to the optical elements and then to the image planes. The origin of the coordinate system in "RAY" lies at the center of the source, the optical element, and the image planes, respectively. The z-axis indicate the forward direction of the central ray and the x-axis is perpendicular to the plane of reflection. The y-axis is always along the normal to the center of the optical element. The plane of reflection or dispersion is, thus, always the y-z plane. The surface of the optical elements always the x-z planes.

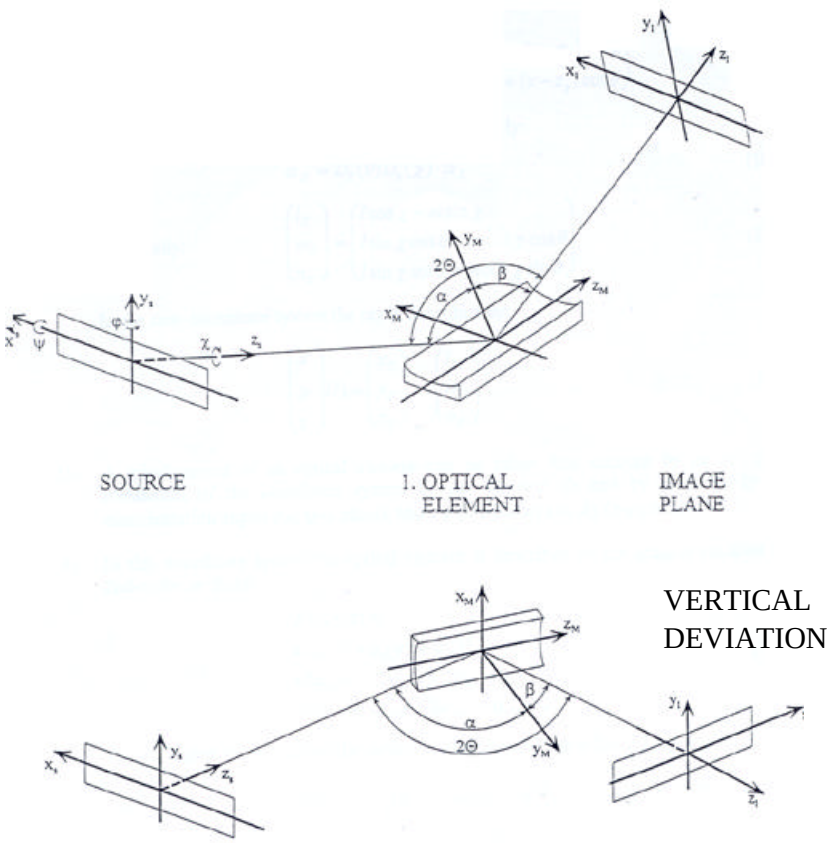

Figure 3.1: *Coordinate systems and angles used in RAY* [Schäfers, 1996]

The flow chart of "RAY", the ray tracing program to simulate the optical system, is shown in figure 3.2.

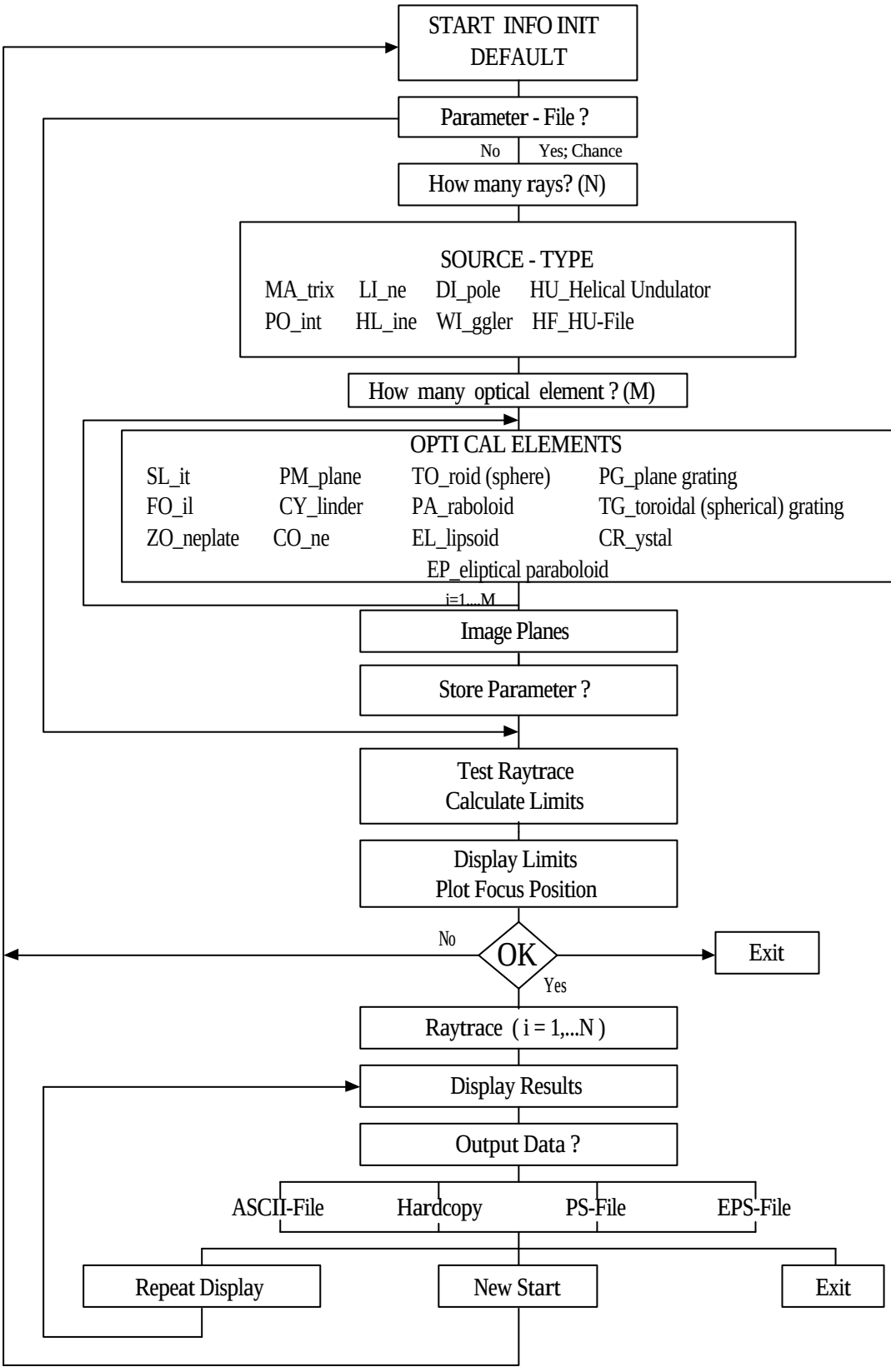

Figure 3.2: *The flow chart of RAY*

The first step of using a ray tracing program for the evaluation of the spectrometer is to choose the number of rays for ray tracing simulation and it should be as large as possible. The larger number of rays will give better statistics while doing analysis (Maximum no of Rays is 9999999 only and is limited by the computational power of the computer). This program is installed on an Alpha Server 4100 computer system with Open VMS operating system. In our case 3000000 rays are used in general for simulation. This spectrometer will be used as the secondary monochromator to resolve the soft X-ray fluorescence emitted by exciting a sample using the monochromatized light from the photoemission beamline. The size of the image at the sample position is 1.08 x 0.65 mm^2 (the standard deviation equal 0.437 mm in horizontal direction and equal 0.299 mm in vertical direction). This information is useful in the deciding the type of the source to be used in the ray tracing. Therefore, the source was assumed as a point source with gaussian distribution which have standard deviation equal to 0.2 mm both in the width and height directions. The optimum divergences of the source used in the horizontal direction and the vertical direction are 30 mrad. The other parameter in this step is the photon energy and it can be varied from 50 eV to 1000 eV. Next step is to decide the number of optical elements to be used in a simulation and in the case of our spectrometer these are three elements (two slit and spherical grating).

The first optical element is the entrance slit (S1). The image width size is limited by the slit width of the entrance slit. In this case the image should not larger than 40 mm wide because the size of the detector is 40x40 mm^2. Thus the entrance slit width is set equal to 1.5 mm. The slit height can be varied from 0-100 μ m. Distance of the source from the slit is to be added in this step for defining the first optical element entrance slit position. The next optical element is the spherical grating. The size of the grating, line density, the radius, the distance from the entrance slit (entrance arm length) and the profile (blazing parameters) should be supplied to the ray tracing program in defining the grating (optical element #2). After we put all of parameter about the grating, the ray tracing program will calculate the grating efficiency. The third optical element is the exit slit (S2) and exit slit parameters should be given in. The incidence angle is fixed for each grating but the diffraction angle will vary for each photon energy. The parameters of exit slit also should be

varied like in the case of entrance slit i.e. the slit width will be fixed and height will be varied.

After supplying the information, the Ray tracing program will calculate the limits of the parameters in this step and we can choose whether we want to continue, or not. In case of a problem we will start this program again but if we want to continue this program will simulate and show the data of all optical elements, the spot diagram showing the ray distribution, energy distribution, angular distribution, the intensity distribution, the number of reflected rays and the flux. The data that we get from the simulation will tell us the results in detail. By finding the optimum value from this, we can finalize the design to give a good efficiency.

By using the design criteria and the methodology mentioned in this chapter the soft X-ray spectrometer can be designed. To obtaining the final parameters of the design, the detailed analysis of the results at each step will play an important role. The details of the results obtained stage by stage, the analysis of the results and the final specifications of the spectrometer are described in the following chapter.

Chapter IV

Results and Discussion

The spectrometer under consideration should cover the energy range of 50-1000 eV. The expected average resolving power of the spectrometer is about 700. The spectrometer will use the Rowland geometry to obtain high resolution over the large energy range and will use three spherical gratings to cover the region efficiently. The details of design evaluation and results obtained will be discussed in this chapter. It should be mentioned that the results presented in the form of graphs and spot diagrams shown in this chapter are obtained using the software package Microsoft Excel (version 8.0) and similarly for the data obtained from the calculations and simulations.

4.1 Analytical Calculation

4.1.1 Deviation Angle

For a given spectrometer geometry the deviation angle is the sum of angle of incidence and diffraction angle (α-β). By using the grating equation 2.1, one can obtain the range of angle of incidence α to be used to design the spectrometer. This range will help in deciding the deviation angle range to used for selecting the deviation angle. The Soft X-ray spectrometer will use very low values of angle of incidence. The variation of reflectance of a grating in the energy range 50-1000 eV for various α values in the range of 1°-10° is calculated by using a program called "REFLEC" [Schäfers and Krumrey, 1996]. The results obtained are shown in the Figure 4.1.

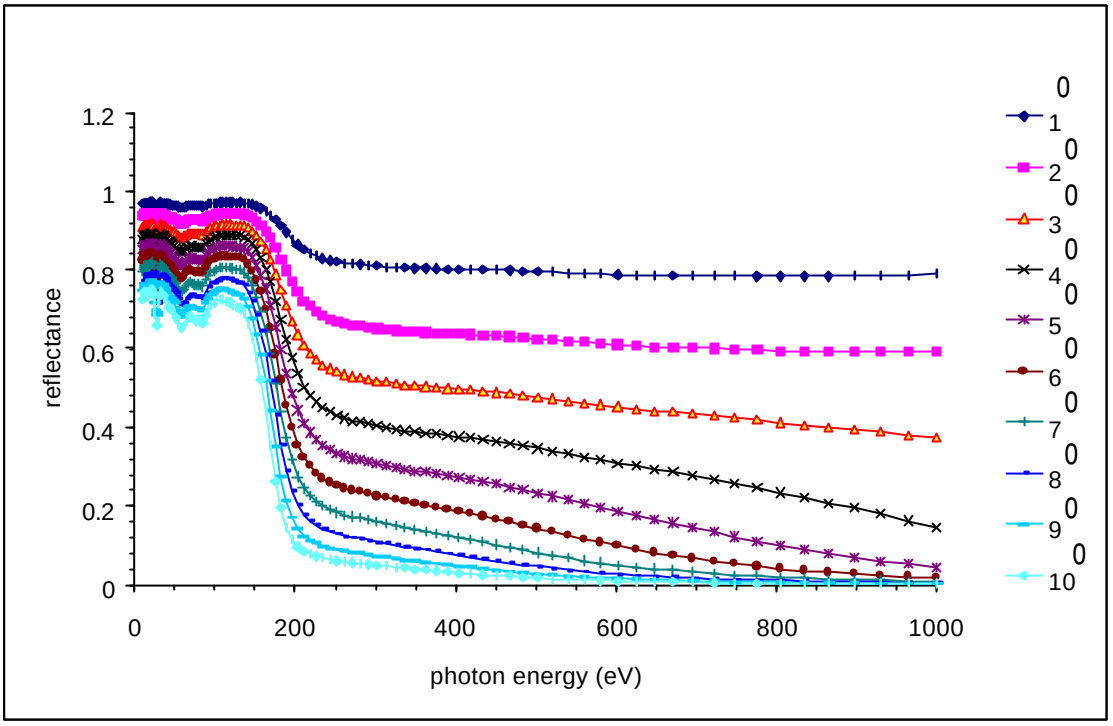

Figure 4.1: *Variation of the Reflectance of the spherical grating with various grazing incidence angles from 1° to 10° degree*

The above Figure shows the variation of the reflectivity of the grating in the range of the small grazing angle (the large angle of incidence). From this one can chose the range of angle of incidence to find the optimum angle of incidence for the grating. In the next step the relation between deviation angle and the line density of the gratings to be used in the spectrometer is obtained. By the variation of the line density of gratings, the line density and the deviation angle which give the high efficiency were determined.

4.1.2 Line Density

The efficiency of a grating depends on the groove density also a part of deviation angle. One can calculated the efficiency of the gratings for a given fixed line density over a photon energy region of interest. Figure 4.2 show the relationship between the efficiency of the gratings with photon energy for difference line densities. From the Figure 4.2a to 4.2c it is clear that as we increase the deviation angle the efficiency curve become broader in a large energy range with reduced peak value of efficiency.

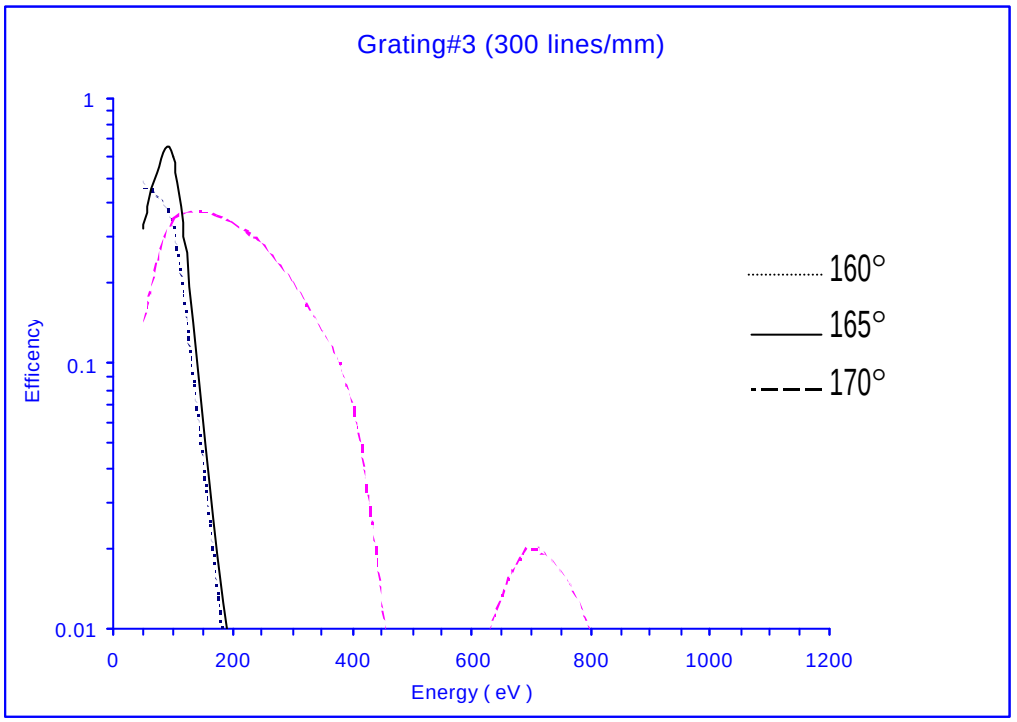

Figure 4.2.a: *Variation of the efficiency of a (300 lines/mm) spherical grating at various deviation angles*

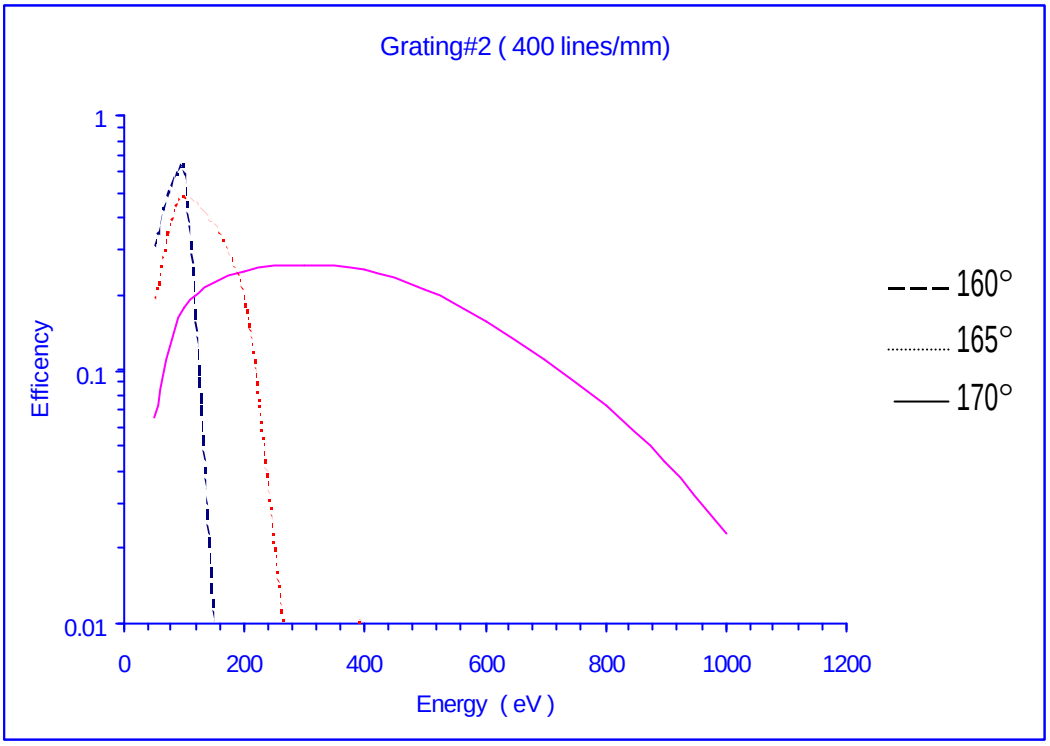

Figure 4.2.b: *Variation of the efficiency of a (400 lines/mm) spherical grating at various deviation angles*

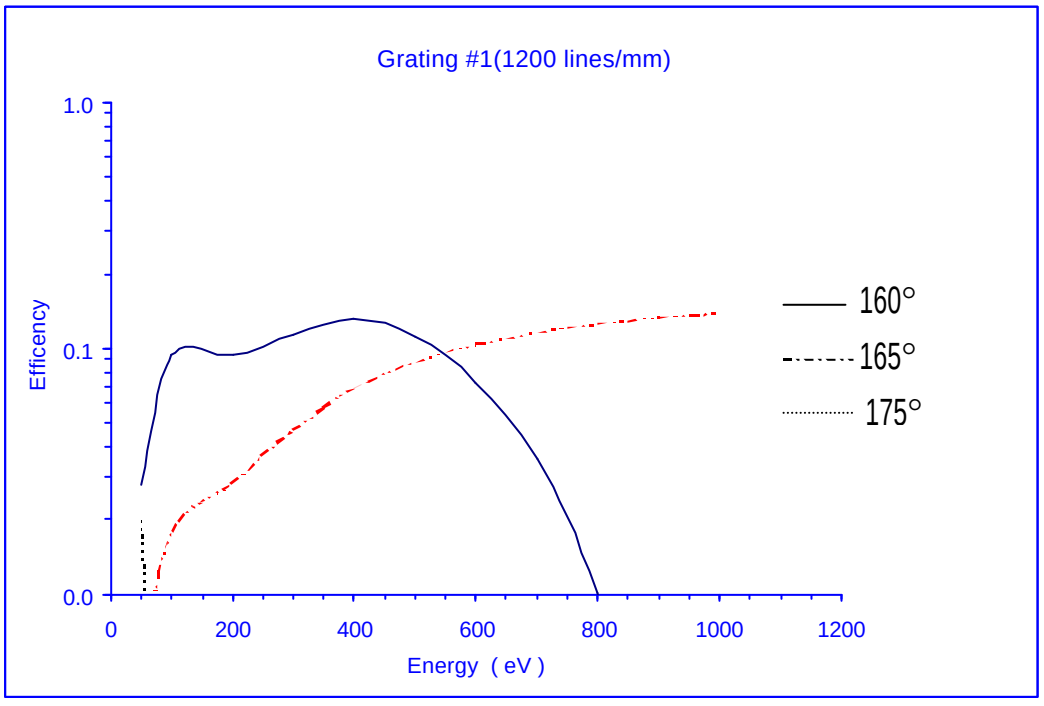

Figure 4.2.c: *Variation of the efficiency of a (1200 lines/mm) spherical grating at various deviation angles*

From Figure 4.2a for grating #3 (line density of 300 line/mm), a deviation angle (α-β) of 165° gives a high reflectivity in the range of photon energy 50 to 200 eV. From Figure 4.2b, for grating #2 (line density of 400 line/mm), a deviation angle of 170° gives a high reflectivity in the range of photon energy 200 to 500 eV. From Figure 4.2c for grating #1 (line density of 1200 line/mm), a deviation angle of 165° gives a high reflectivity in the range of photon energy 400 to 1000 eV. From the efficiency data it is obvious that unless we use three gratings in the spectrometer, we can not cover the energy range satisfactorily.

4.1.3 Blaze Angle

Because we use blazed gratings in this design, an appropriate blaze angle for the gratings should be found and it is done in this step. Since three gratings are used in the spectrometer, one has to fine the blaze angle for each of the grating. For calculation of efficiency one can used a program in "RAY". For finding the blazing angle range, one can calculated the efficiency of the gratings with variations of blaze angles and plotted the efficiency data in Figure 4.3.a to 4.3.c. From Figures 4.3a, 4.3b and 4.3c, one can select the blaze angle that give the high efficiency for each grating. From these figures one can fine the range of the blaze angle.

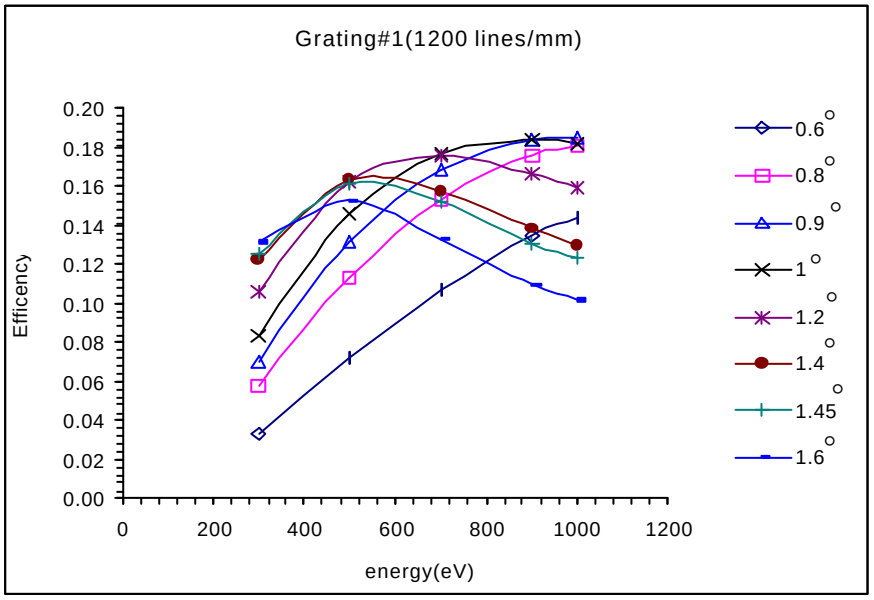

Figure 4.3.a: *Variation of the reflectance of grating #1 with blazed angle*

To find the exact value of the blaze angle, one can evaluated the relationship between the efficiency of the grating and the blaze angles of the three gratings, at a specific photon energy for each grating. The photon energies at which the relationship between efficiency of grating and the blaze angle obtained are, 400 eV, 280 eV and 100eV for grating #1 grating #2 and grating #3 respectively.

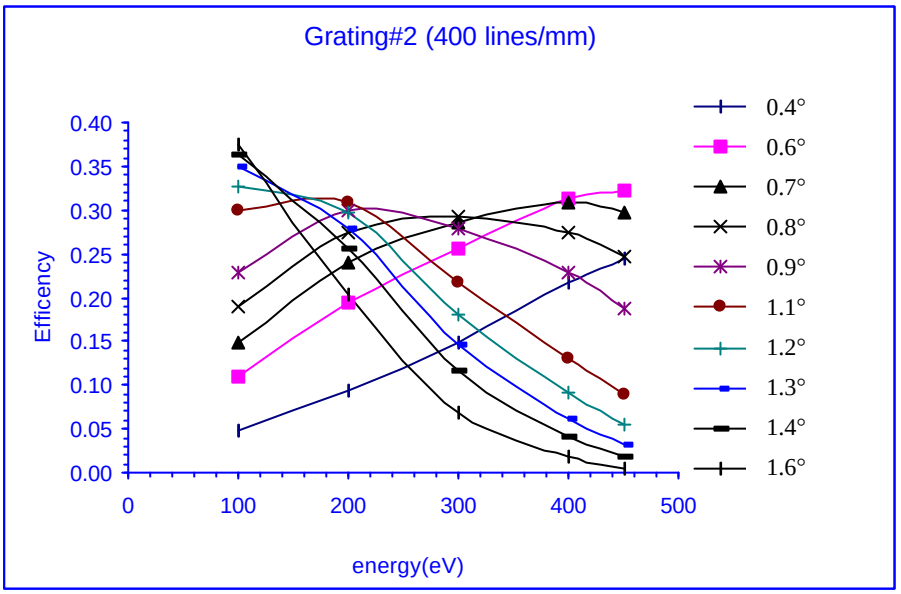

Figure 4.3.b: *Variation of the reflectance of grating #2 with blazed angle*

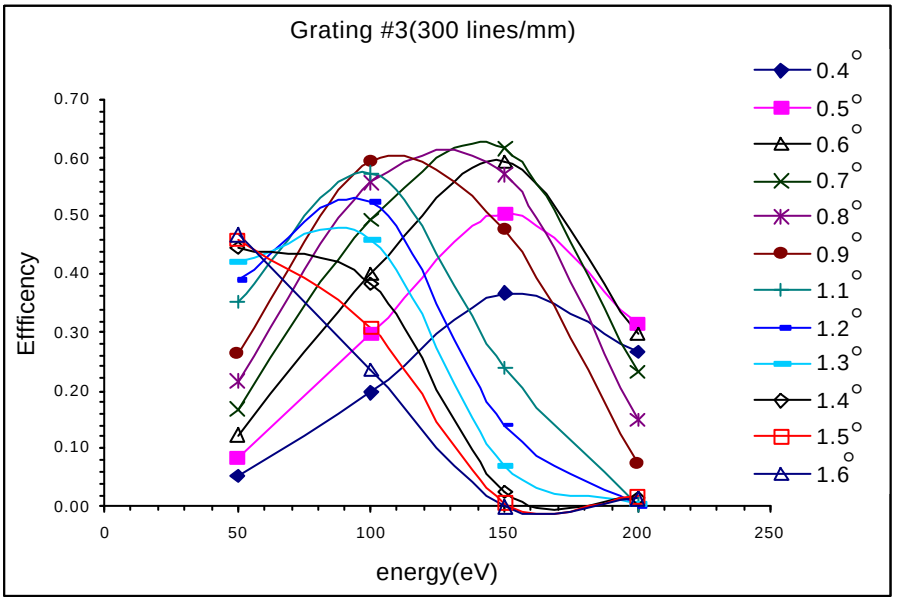

Figure 4.3.c: *Variation of the reflectance of grating #3 with blazed angle*

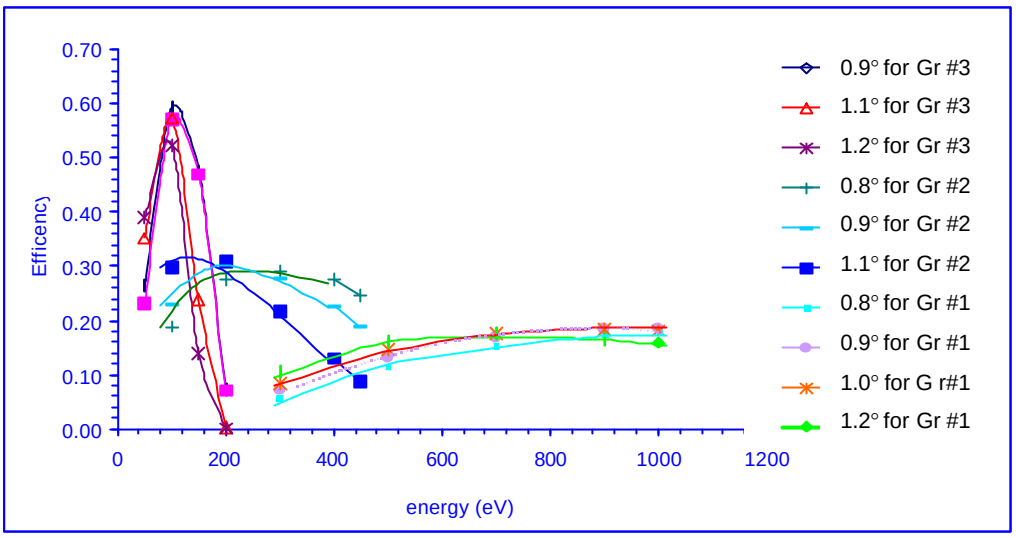

Figure 4.3.d: *Comparison of the variation of the efficiency of three spherical gratings #1, #2 and #3 with blaze angle*

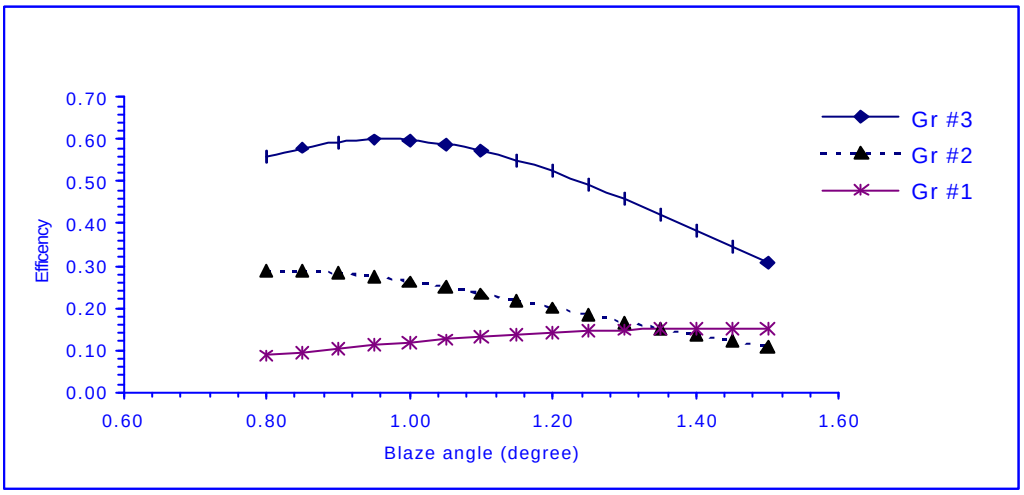

Figure 4.4: *Comparison of the efficiency of three gratings that gratings #1, #2 and #3 at photon energies 400 eV, 280 eV, and 100 eV respectively with blaze angle*

From Figure 4.4, the optimum blaze angle for grating #1, grating #2 and grating #3 are obtained and they are 1.47°, 0.82° and 0.92°. The blaze angles were calculated using equation 2.11 for each grating also. The results of this are shown for comparison in table 4.1. This blaze angle will be used for exact ray tracing later.

Table 4.1: Blaze angle from graph and from calculation.

grating number	blaze angle from graph	blaze angle from calculation
1	1.47°	1.50°
2	0.82°	0.84°
3	0.97°	0.96°

4.1.4 The Spectrometer Layout

Using the results of the calculation performed the parameters needed for the design of the spectrometer are obtained. The required spectrometer is based on Rowland circle geometry. This spectrometer uses three fixed gratings and a fixed entrance slit. The detector is movable in the normal plane of the slit and gratings, and rotable with a rotation axis through the detector centre and perpendicular to the normal plane. We plan to use either multichannel plate in this spectrometer for the detection of photons. The layout of the spectrometer is shown in the Figure 4.5.

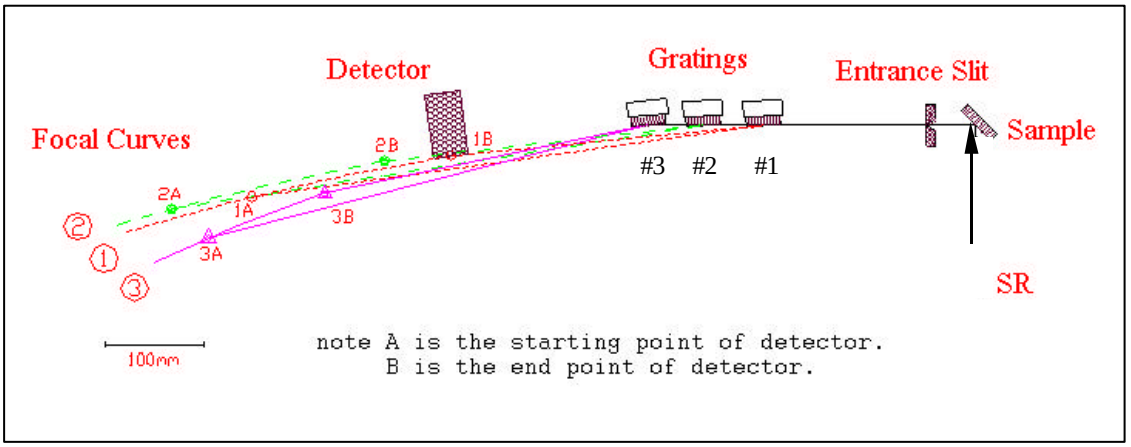

Figure 4.5: *The layout of the required spectrometer*

Table 4.2: The optical parameters of the planned soft X-ray spectrometer

Parameters	Grating# 1		Grating#2		Grating#3	
Grating radius (mm)	5000		5000		3000	
Line density (lines/ mm)	1200		400		300	
Angle of incidence (degree)	88.1		87.4		84.6	
Energy range (eV)	300-1000		100 - 450		50 - 200	
Photon energy (eV)	300	1000	100	450	50	200
Wave length (Å)	41.32	12.396	123.960	27.547	247.92	61.98
Order of diffraction	1		1		1	
Entrance arm length (mm)	165.78		226.82		282.32	
Entrance slit width (μm)	variable from 10 to 100					
Distance sample to entrance slit (mm)	30					
Energy resolution (eV)	0.240	2.669	0.080	1.621	0.044	0.712
Detector size (mm^2)	40 x 40					

Table 4.2 gives the parameters of the required spectrometer. Form this table it has to be noted that the spectrometer consists of three spherical gratings and each grating will cover different energy ranges.

4.1.5 Diffraction Angle and Exit Arm Length

By using the spectrometer layout, the parameters obtained in earlier sections of this Chapter and grating equation 2.1, one can calculated the diffraction angle (β) for each photon energy. After calculating the diffraction angle (β), one can calculated exit arm length by using equation 2.25. The results of these calculations are shown in the table 4.3a for grating #1, Table 4.3b for grating #2 and the table 4.3c for grating #3. The same results are shown in the Figure 4.5a and 4.5b indicating the relationship of the photon energy with diffraction angle and the exit arm length respectively.

Table 4.3.a: The variation of diffraction angle and exit arm length for the grating #1 with each photon energy or wavelength

Incident angle equal 88.1degrees		Entrance arm length equal 165.776 mm	
Photon energy (eV)	Wavelength (Å)	Diffraction angle (degrees)	Exit arm length (mm)
300	41.3	83.98	521.27
350	35.4	84.38	486.49
400	31.0	84.70	458.67
450	27.5	84.97	435.80
500	24.8	85.19	416.59
550	22.5	85.38	400.20
600	20.7	85.54	386.02
650	19.1	85.68	373.59
700	17.7	85.81	362.60
750	16.5	85.92	352.79
800	15.5	86.02	343.98
850	14.6	86.11	336.03
900	13.8	86.20	328.80
950	13.1	86.27	322.19
1000	12.4	86.34	316.11

This table shows the diffraction angle and exit arm length for the grating #1 which has a radius equal to 5 meter and have the line density of 1200 lines/mm.

Table 4.3.b: The variation of diffraction angle and exit arm length for the grating #2 with photon energy or wavelength

Incident angle equal 87.4 degrees Entrance arm length equal 226.815 mm			
Photon energy (eV)	Wavelength (Å)	Diffraction angle (degrees)	Exit arm length (mm)
100	124.0	83.73	546.05
125	99.2	84.27	498.88
150	82.6	84.66	464.76
175	70.8	84.96	438.76
200	61.9	85.20	418.18
225	55.1	85.39	401.44
250	49.6	85.55	387.53
275	45.1	85.68	375.76
300	41.3	85.80	365.66
325	38.1	85.90	356.89
350	35.4	85.99	349.21
375	33.1	86.07	342.40
400	31.0	86.14	336.33
425	29.2	86.20	330.88
450	27.5	86.26	325.97

This table shows the diffraction angle and exit arm length of grating #2 which has a radius equal to 5 meter and have the line density of 400 lines/mm.

Table 4.3.c: The variation of diffraction angle and exit arm length for the grating #3 with photon energy and or wavelength

Incident angle equal 84.6 degrees Entrance arm length equal 282.325 mm			
Photon energy (eV)	Wavelength (Å)	Diffraction angle (degree)	Exit arm length (mm)
50	247.9	81.16	460.80
60	206.6	81.63	436.21
70	177.1	81.99	417.74
80	154.9	82.27	403.33
90	137.7	82.49	391.75
100	123.9	82.68	382.22
110	112.6	82.83	374.24
120	103.3	82.96	367.46
130	95.3	83.07	361.62
140	88.5	83.17	356.54
150	82.6	83.26	352.078
160	77.5	83.33	348.12
170	72.9	83.40	344.59
180	68.9	83.46	341.43
190	65.2	83.52	338.57
200	61.9	83.56	335.98

This table shows the diffraction angle and exit arm length of grating #3 which has a radius equal 3 meter and have the line density of 300 lines/mm.

Using the data from three tables one can plotted the graphs to compare the relationship between the diffraction angle and the exit arm length of all gratings.

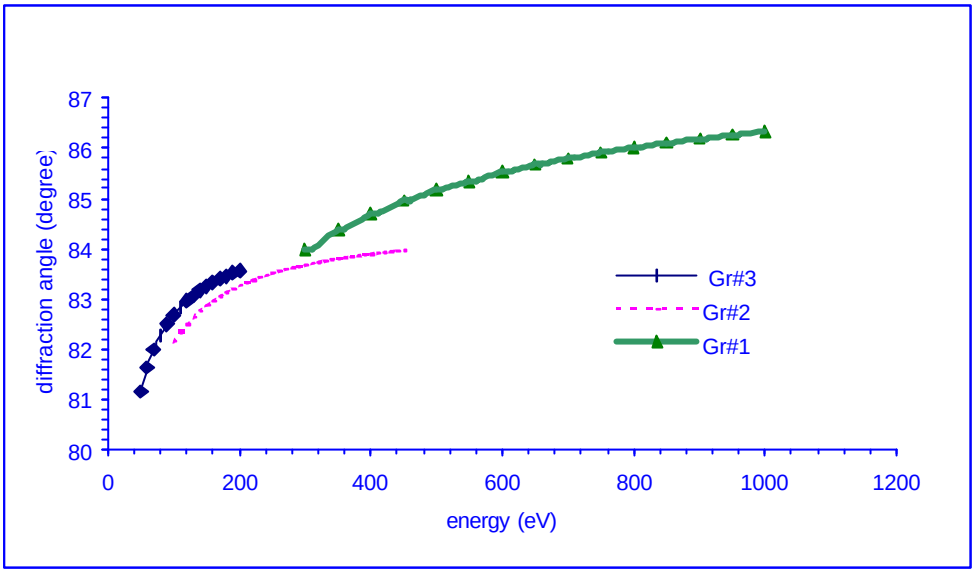

Figure 4.6.a: *The variation of the diffraction angle with photon energy for gratings #1, #2 and #3*

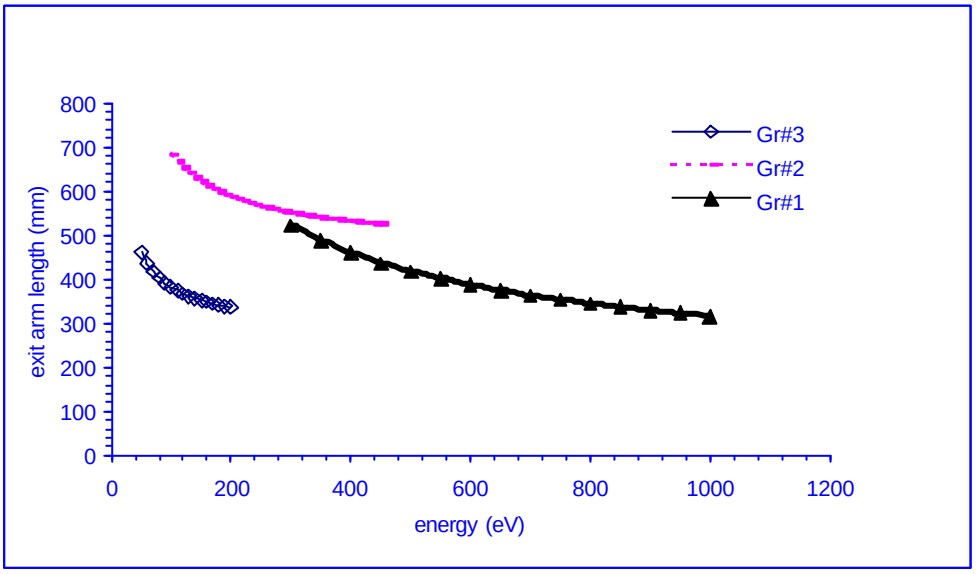

Figure 4.5.b: *The variation of the exit armlength with the photon energy for gratings #1, #2 and #3*

From Figure 4.5 we find that the diffraction angle will increase with photon energy while the exit arm length decrease. Since this spectrometer is using Rowland circle geometry one can calculated the resolution of this spectrometer by using

equation 2.19. By varying the size of the exit slit for each photon energy, one can calculated the resolution for all the gratings and the results obtained are shown in Table 4.4a, 4.4b, 4.4c for grating #3, grating #2 and grating #1. The same were shown in the form of single graph for comparison in Figure 4.7.

Table 4.4.a: The resolution of grating #3 over the energy range 50-200 eV

Photon Energy (eV)	Resolution (eV)		
	Exit slit=0.02mm	Exit slit=0.05mm	Exit slit = 0.10mm
50	0.045	0.111	0.222
75	0.100	0.250	0.500
100	0.178	0.445	0.890
125	0.278	0.695	1.390
150	0.400	1.001	2.002
175	0.545	1.362	2.724
200	0.712	1.779	3.558

Table 4.4.b: The resolution of grating #2 over the energy range 100-400 eV

Photon Energy (eV)	Resolution (eV)		
	Exit slit=0.02mm	Exit slit = 0.05mm	Exit slit = 0.10mm
100	0.080	0.200	0.400
150	0.180	0.450	0.901
200	0.320	0.801	1.601
250	0.500	1.251	2.502
300	0.721	1.801	3.603
350	0.981	2.452	4.904
400	1.281	3.202	6.405
450	1.621	4.053	8.106

Table 4.4.c: The resolution of grating #1 over the energy range 300-1000 eV

Photon Energy (eV)	Resolution (eV)		
	Exit slit=0.02 mm	Exit slit = 0.05mm	Exit slit = 0.10mm
300	0.240	0.600	1.201
400	0.427	1.067	2.135
500	0.667	1.668	3.336
600	0.961	2.402	4.804
700	1.308	3.269	6.538
800	1.708	4.270	8.540
900	2.162	5.404	10.809
1000	2.669	6.672	13.344

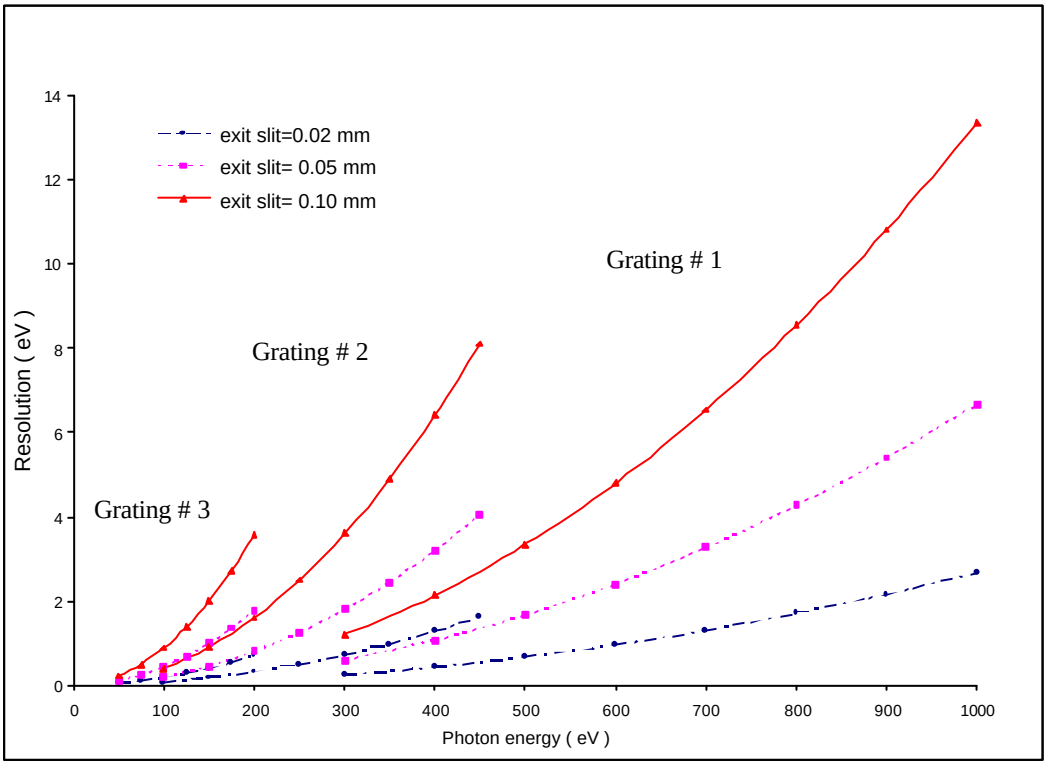

Figure 4.7: *The resolution of spectrometer for gratings #1, #2 and #3 with various exit slit widths*

4.2 Ray Tracing Simulation

After obtaining the layout and the parameters of the spectrometer, the results of the design are evaluated further using ray tracing simulations by performing exact ray tracing. Ray tracing program will be used for this work along with the data obtained in section 4.1.

4.2.1 Grating efficiency

In the beginning, one can used,"RAY", the ray tracing program to find the efficiency of the grating. A sample session of the program with inputs is given in the Appendix. In the efficiency calculation, a part of the ray tracing program starting from step.1 to step.48 described in the Appendix-3 is used. The calculation is repeated for each photon energy (for each grating) by changing the parameters. Then by using Microsoft Excel (version 8.0), one can plotted the data obtained from Ray tracing program. The relationships between the photon energy and the efficiency in for s-polarized and p-polarized light are shown in the figure 4.8a and 4.8b respectively.

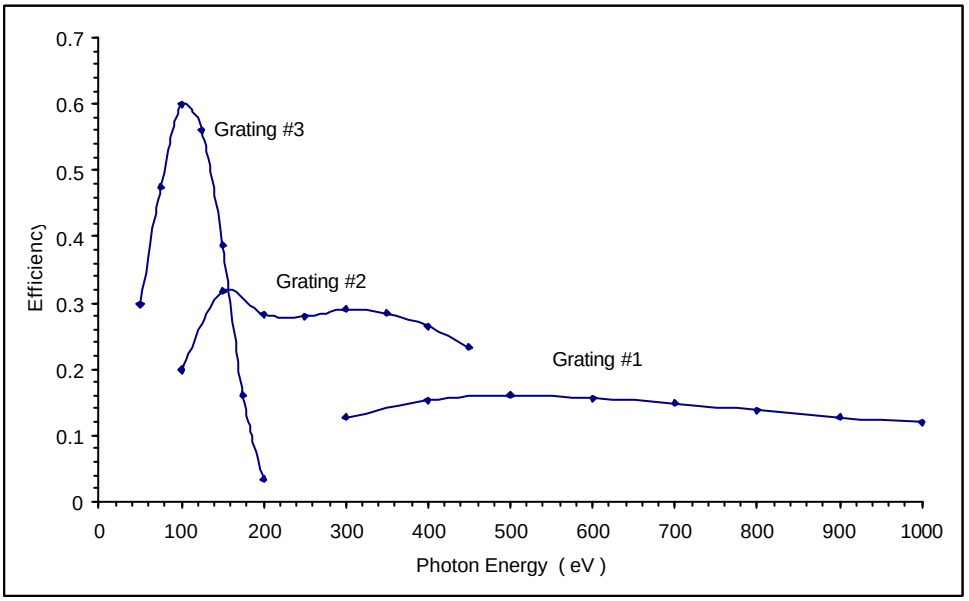

Figure 4.8.a: *Variation of the efficiency of s-polarized light at each grating in the spectrometer*

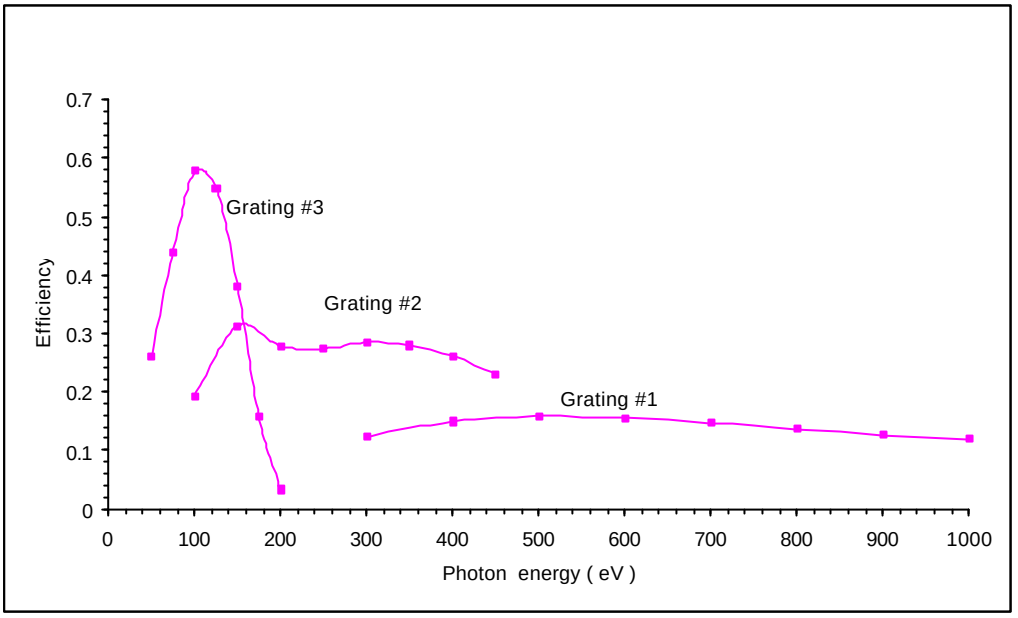

Figure 4.8.b: *Variation of the efficiency of p-polarized light at each grating in the spectrometer*

From these graphs it is clear that the efficiency of the grating for s-polarized light and p-polarized light is the same. The efficiency of the grating #3 has a maximum at photon energy equal 100 eV, for the garting #2 the efficiency is maximum at photon energy equal 150 eV. For the grating #1 the efficiency is almost constant through out the energy range. These graphs will be useful to decide the choice of the grating in the spectrometer while doing experiments. For example if the incoming photon energy is equal 100 eV we should select the grating #3 but if the incoming photon energy is 200 eV we should select grating #2. The next parameter to be determined is the resolution of the spectrometer.

4.2.2 Resolution

The resolution is one of the important parameters of the spectrometer. Even for this, one can used "RAY", the ray tracing program. The steps indicated in the sample session given in the Appendix-2 from beginning to the end are used for this calculation. After the simulation a wide variety of data will be shown in the results including number of the geometric rays, the number of the reflected rays, maximum

flux density and the flux at each optical element. To find the resolution, we should know the energy distribution at the exit slit. The data obtained from ray tracing in form of ray section points at the image position is used in the plotting with the Microsoft Excel. Figure 4.9 shows the relationship between the Intensity (arb. unit) and photon energy (eV). The full width at the half maximum (FWHM) of this intensity distribution at the image position gives the resolution. To get a better statistics for the intensity distribution, the ray tracing should be repeated until sufficient points for plotting are obtained. The resolution of the spectrometer in the case of fixed exit arm length and variable the entrance arm length are shown in the figure 4.10.a, 4.10.b and 4.10.c for grating #1, grating #2 and grating #3 respectively.

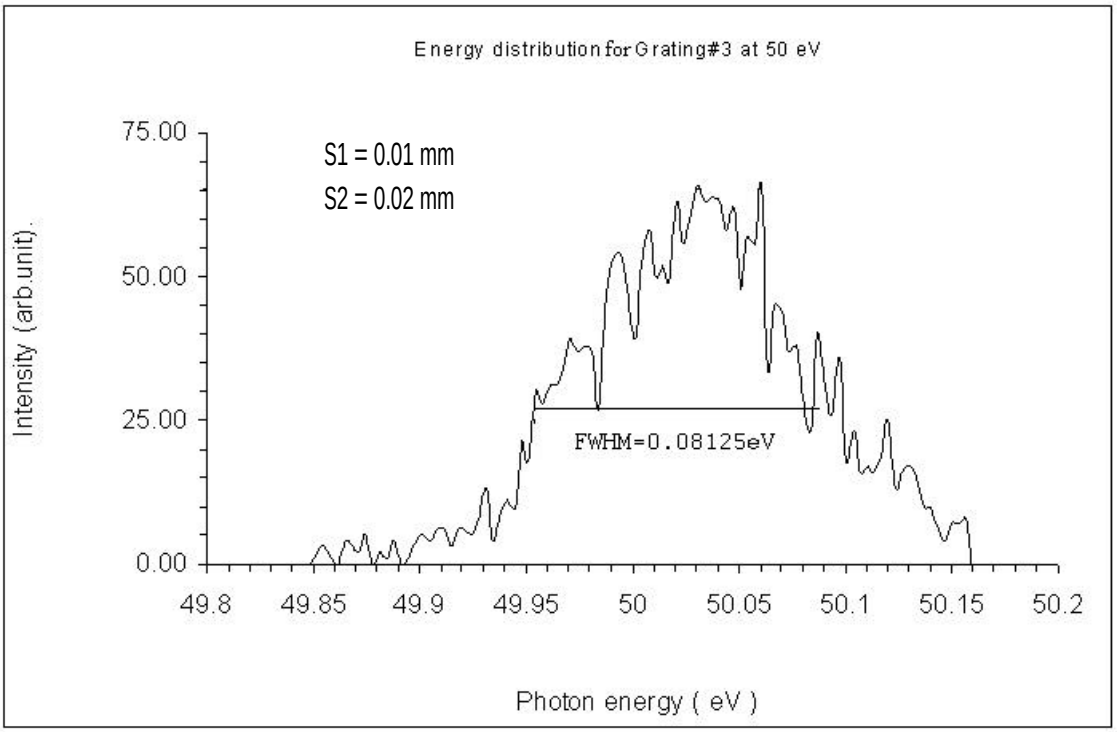

Figure 4.9: *Energy distribution of the image for grating #3 at 50 eV*

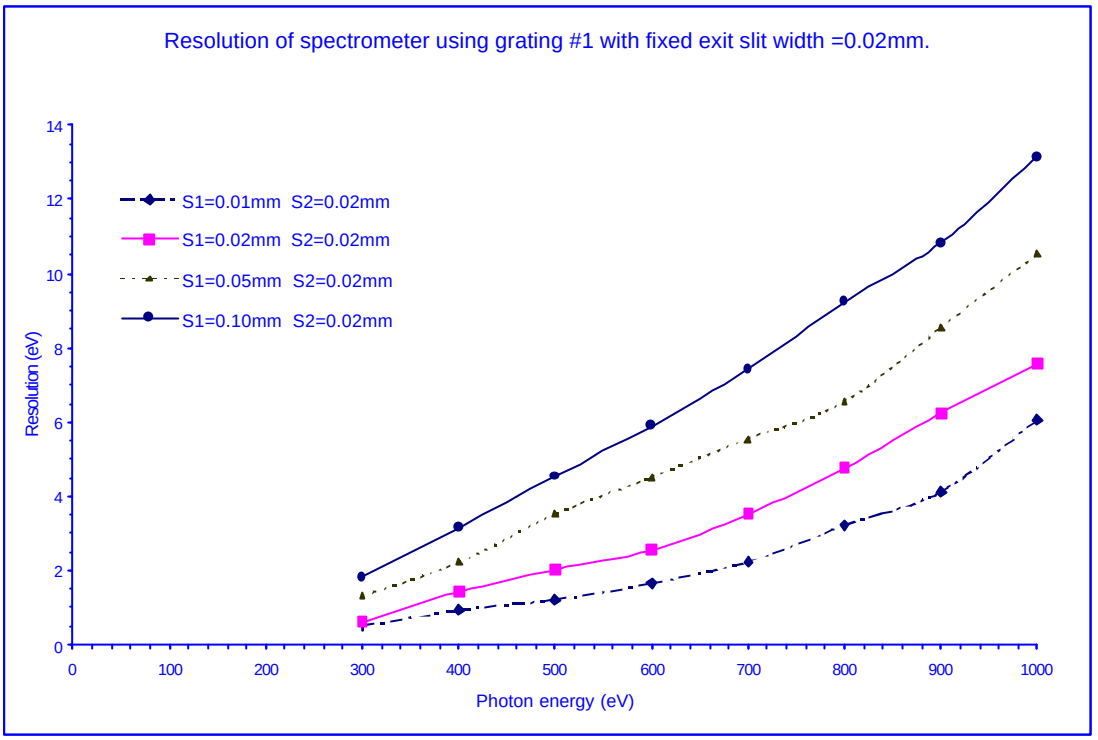

Figure 4.10.a: *Variation of the resolution of the spectrometer for grating #1 with fixed exit slit width and various entrance slit widths*

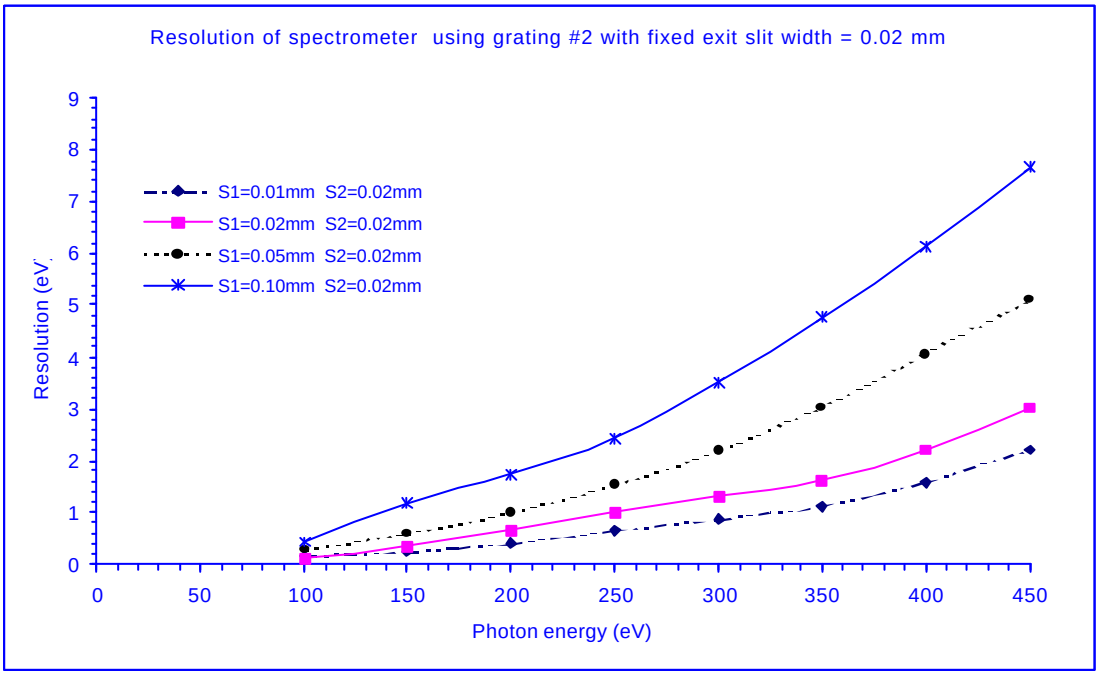

Figure 4.10.b: *Variation of the resolution of the spectrometer for grating #2 with fixed exit slit width and various entrance slit widths*

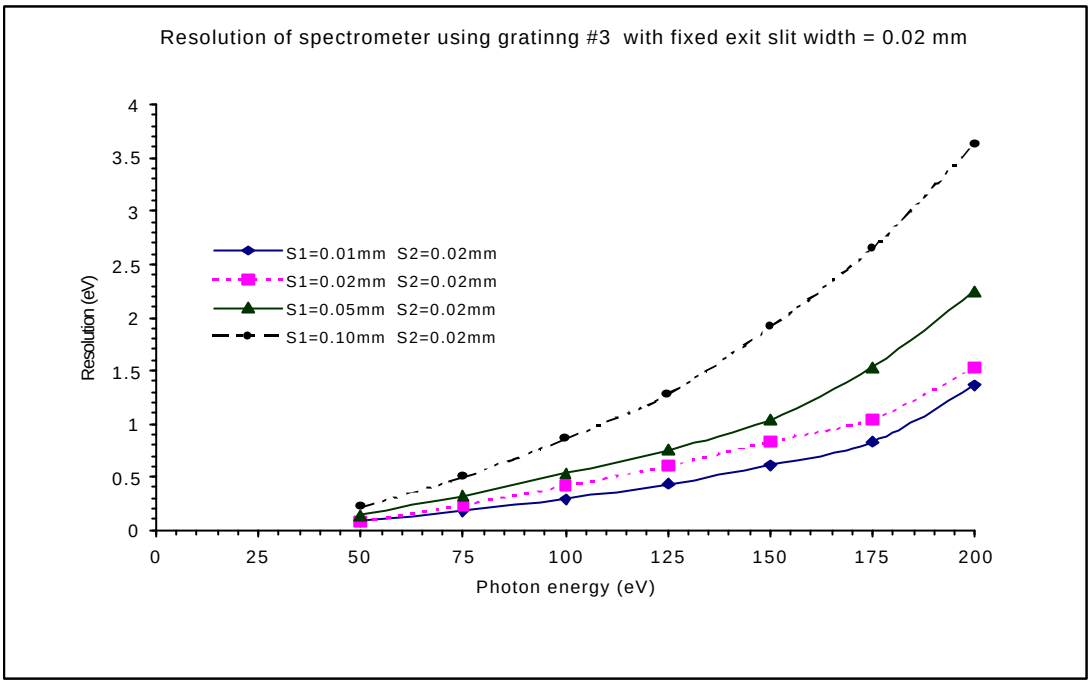

Figure 4.10.c: *Variation of the resolution of the spectrometer for grating #3 with fixed exit slit width and various entrance slit widths*

These three graphs indicate that with the fixed exit slit width the magnitude of resolution (ΔE) will increase with the increasing entrance slit width i.e. the resolving power will go down. Thus for obtaining higher resolving power from the spectrometer we should use small entrance slit widths.

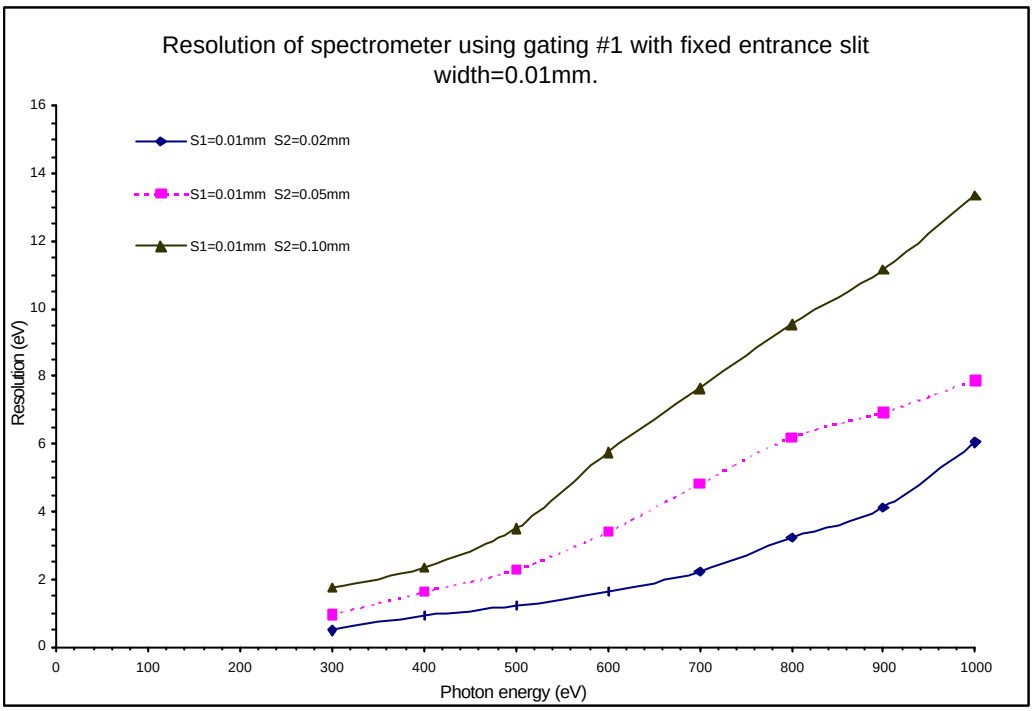

Figure 4.11.a: *Variation of the resolution of the spectrometer using grating #1 with fixed entrance slit width and various exit slit widths*

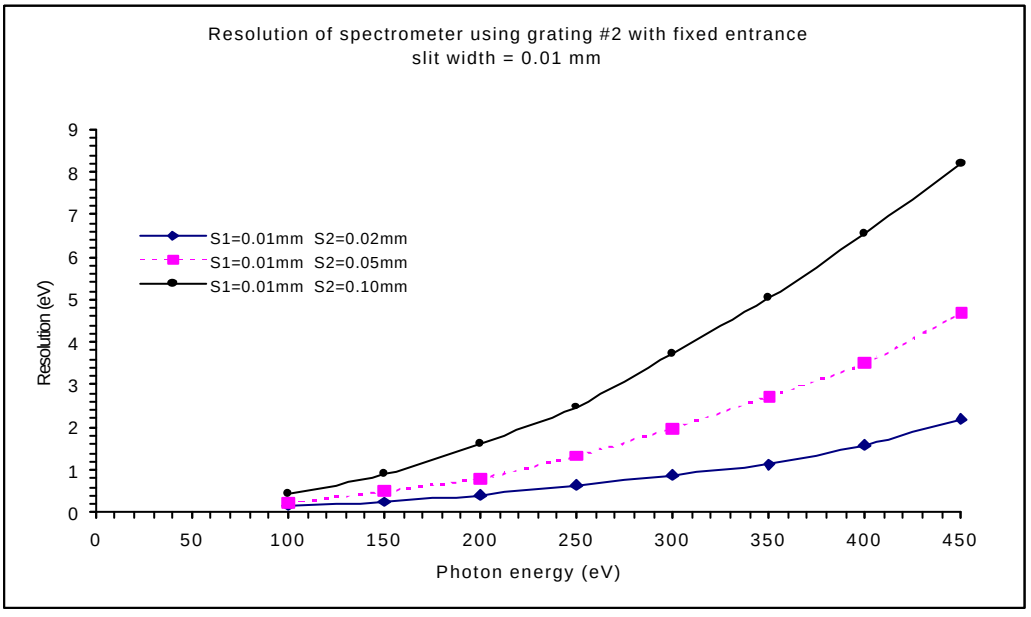

Figure 4.11.b: *Variation of the resolution of the spectrometer using grating #2 with fixed entrance slit width and various exit slit widths*

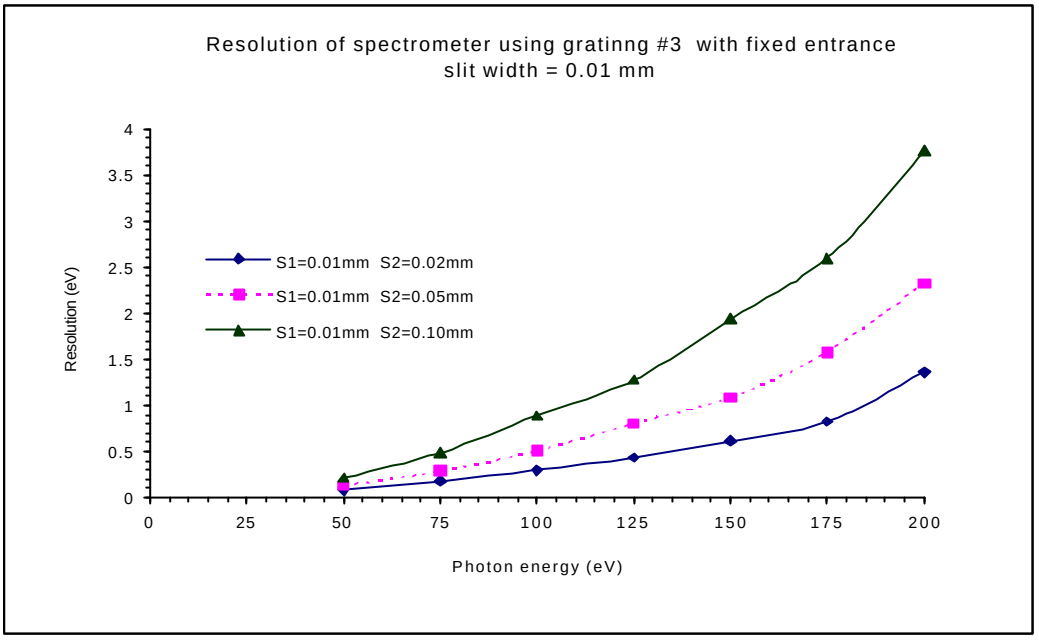

Figure 4.11.c: *Variation of the resolution of the spectrometer using grating #3 with fixed entrance slit width and various exit slit widths*

The results, for three gratings follow the same pattern as the earlier case. For a fixed entrance slit width the magnitude of resolution ΔE increase when the exit slit widths are increased too. For obtaining good resolution from the spectrometer we should use a small opening of exit slit. However it has to be mentioned that the resolution change with entrance slit widths is more drastic than with exit slit widths. Another important parameter that should be determined in the next step is the transmission of the spectrometer.

4.2.3 Transmission

The transmission will tell about the throughput of the spectrometer. The value of the transmission comes from the ratio of the number of the rays passing through at the exit slit to the number of the entering the entrance slit. This fraction will change with the energy, entrance and exit slit widths and heights, diffraction efficiency of the gratings etc. one can obtained the data required for the calculation of transmission of the spectrometer using the ray tracing program "RAY". The method of evaluation is

slightly different from the method of resolution evaluation. Here, we note, the total number of the rays traced through the entrance slit of the spectrometer and the total number of rays going out of the exit slit. By using these numbers, the transmission of spectrometer is calculated. The similar step is repeated by varying different parameters to see their effect on transmission. Transmission data obtained for different energy ranges using different gratings are plotted. Figure 4.12.a, 4.12.b and 4.12.c show transmission of grating #1, grating #2 and grating #3 for fixed exit slit width and with various entrance slit widths. Figure 4.13.a, 4.13.b and 4.13.c show the transmission of grating #1, grating #2 and grating #3 for variable exit slit widths and a fixed entrance slit width.

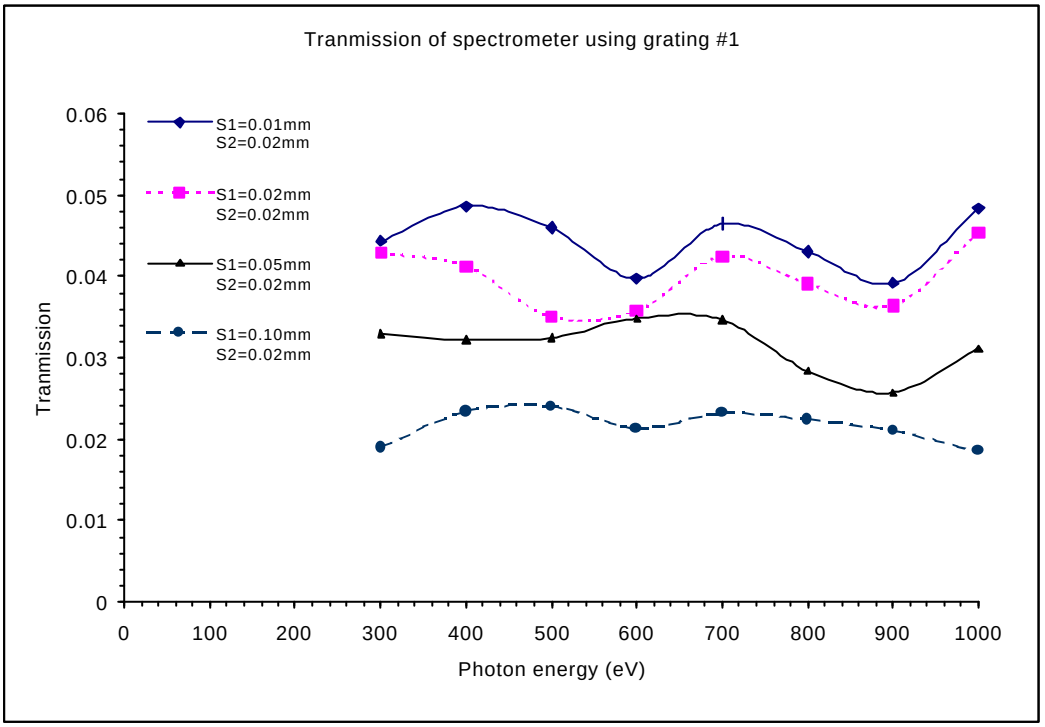

Figure 4.12.a: *Variation of the transmission of the spectrometer using grating #1 with fixed exit slit width and various entrance slit widths*

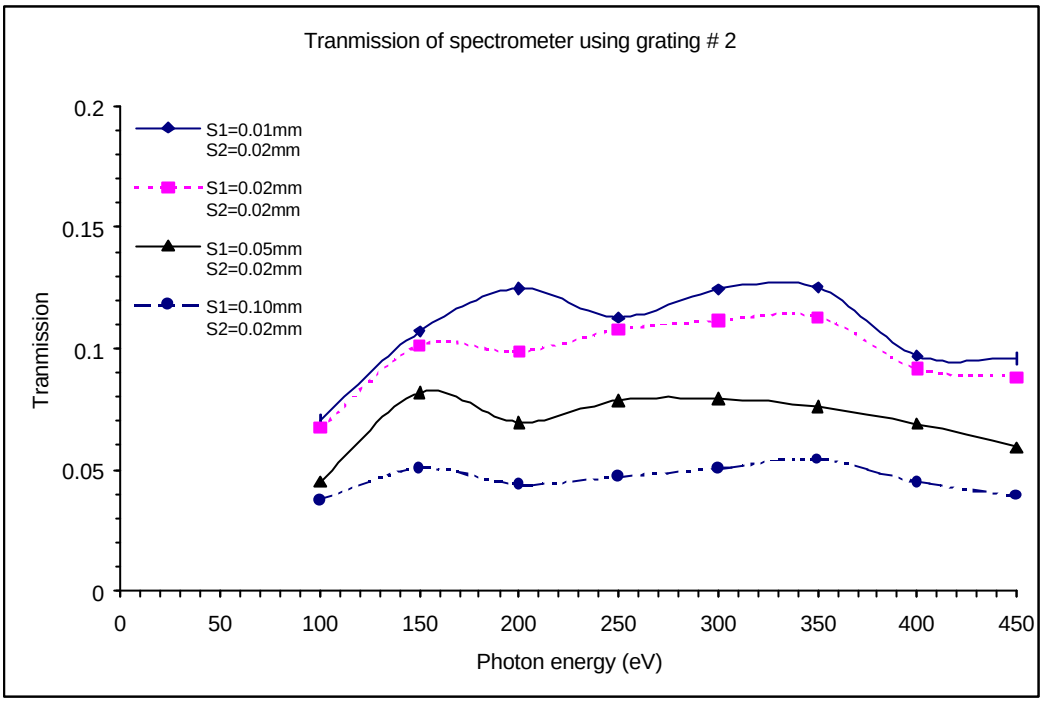

Figure 4.12.b: *Variation of the transmission of the spectrometer using grating #2 with fixed exit slit width and various entrance slit widths*

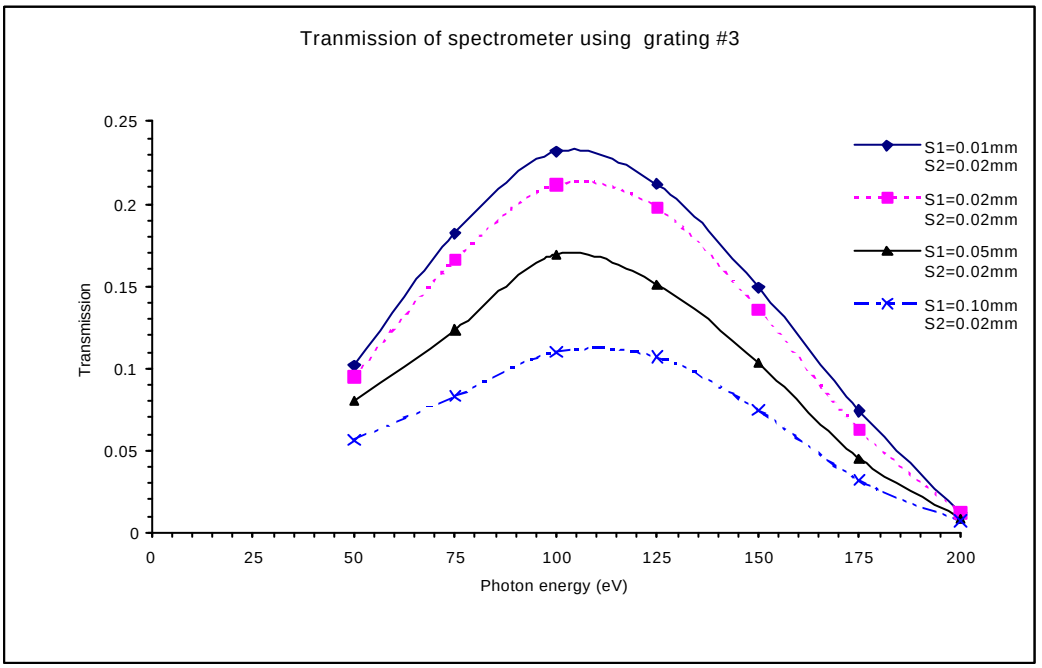

Figure 4.12.c: *Variation of the transmission of the spectrometer using grating #3 with fixed exit slit width and various entrance slit widths*

It is found that transmission of the spectrometer decreases with reducing entrance slit width. Sometimes the size of the slit width which gives the high resolution can not be used because the transmission is very low. The results of the transmission are useful with the consideration of the slit widths. In the next step the entrance slit width is fixed, the exit slit width is varied in the similar way to see the trend of the transmission of the spectrometer for each grating.

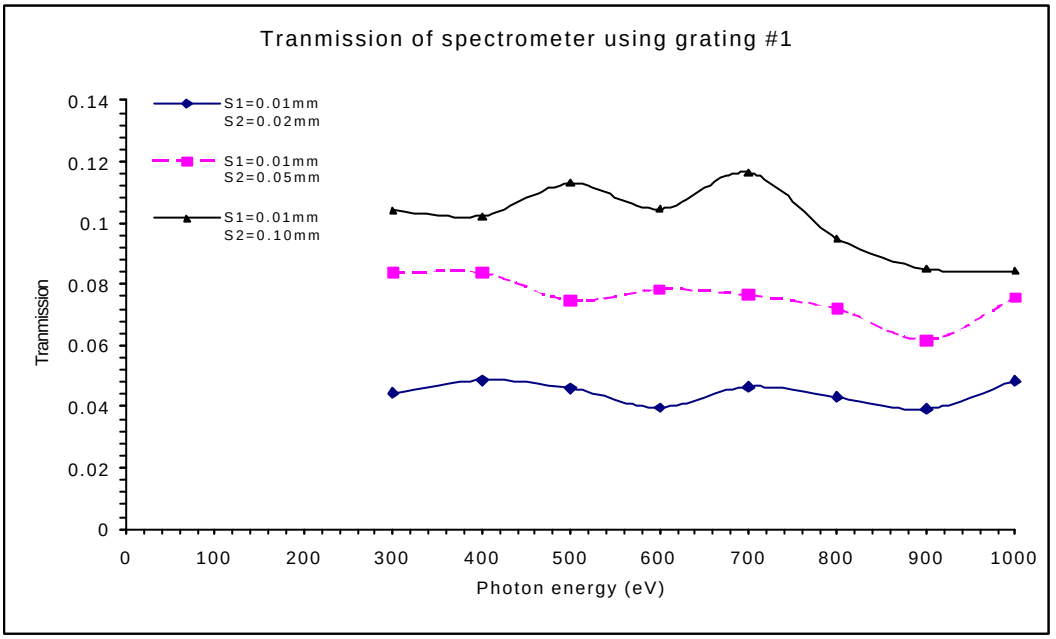

Figure 4.13.a: *Variation of the transmission of the spectrometer using grating#1 with fixed entrance slit width and various exit slit widths*

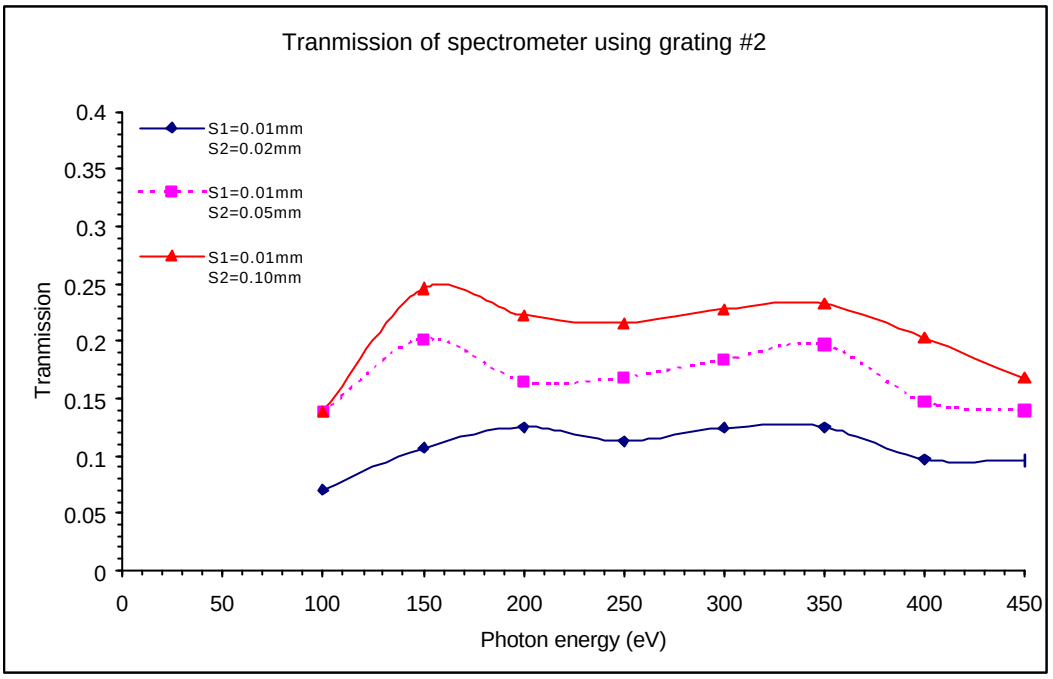

Figure 4.13.b: *Variation of the transmission of the spectrometer using grating #2 with fixed entrance slit width and various exit slit widths*

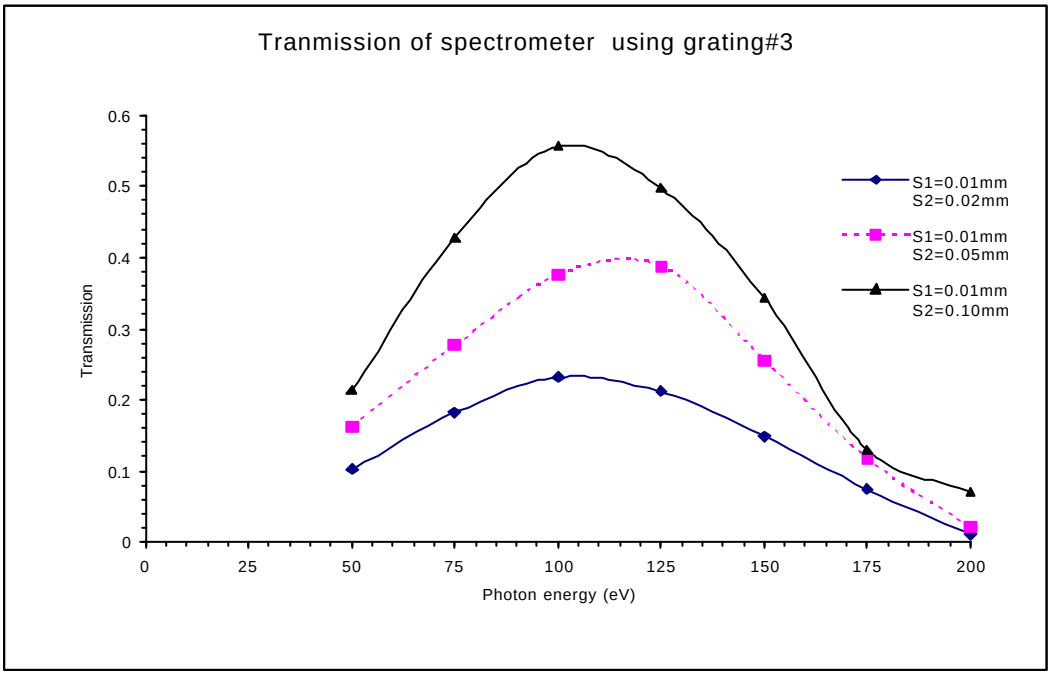

Figure 4.13.c: *Variation of the transmission of the spectrometer using grating #3 with fixed entrance slit and various exit slit widths*

In this case the transmission will increase when the exit slit is increased. When the entrance slit equal to 0.01 mm and the exit slit equal to 0.02 mm, the spectrometer will give the best resolution but the transmission will be very low. We should select the size of the slit width that give the high resolution but the flux of the reflected photon should be enough for the detector to detect. In the experiments we should select the size of the slit width that give the high flux of the photons after that we should increase the size of the slit width wide enough to obtain the required resolution.

4.2.4 Spot Diagram

Now we know about the resolution and the transmission of the spectrometer. We use the same ray tracing method to find the data required for plotting spot diagram to show the nature and size of the image in the image plane for this spectrometer. The spot diagrams are plotted using the results of ray tracing performed as explained in appendix-2 with help of Microsoft Excel program. The details of the spot diagrams are given in the table 4.7 and the sport diagrams are shown in Figure 4.14.

Table 4.7: The FWHM of the image size from the spectrometer using three gratings with various entrance slit widths

		The image size in vertical direction when the entrance slit width equal (mm)			
Grating number	Photon Energy (eV)	0.01 mm	0.02 mm	0.05 mm	0.10 mm
3	50	0.049	0.061	0.062	0.088
	100	0.047	0.049	0.058	0.087
2	100	0.176	0.179	0.187	0.206
	300	0.079	0.08	0.088	0.105
1	300	0.074	0.077	0.092	0.107
	1000	0.083	0.089	0.096	0.119

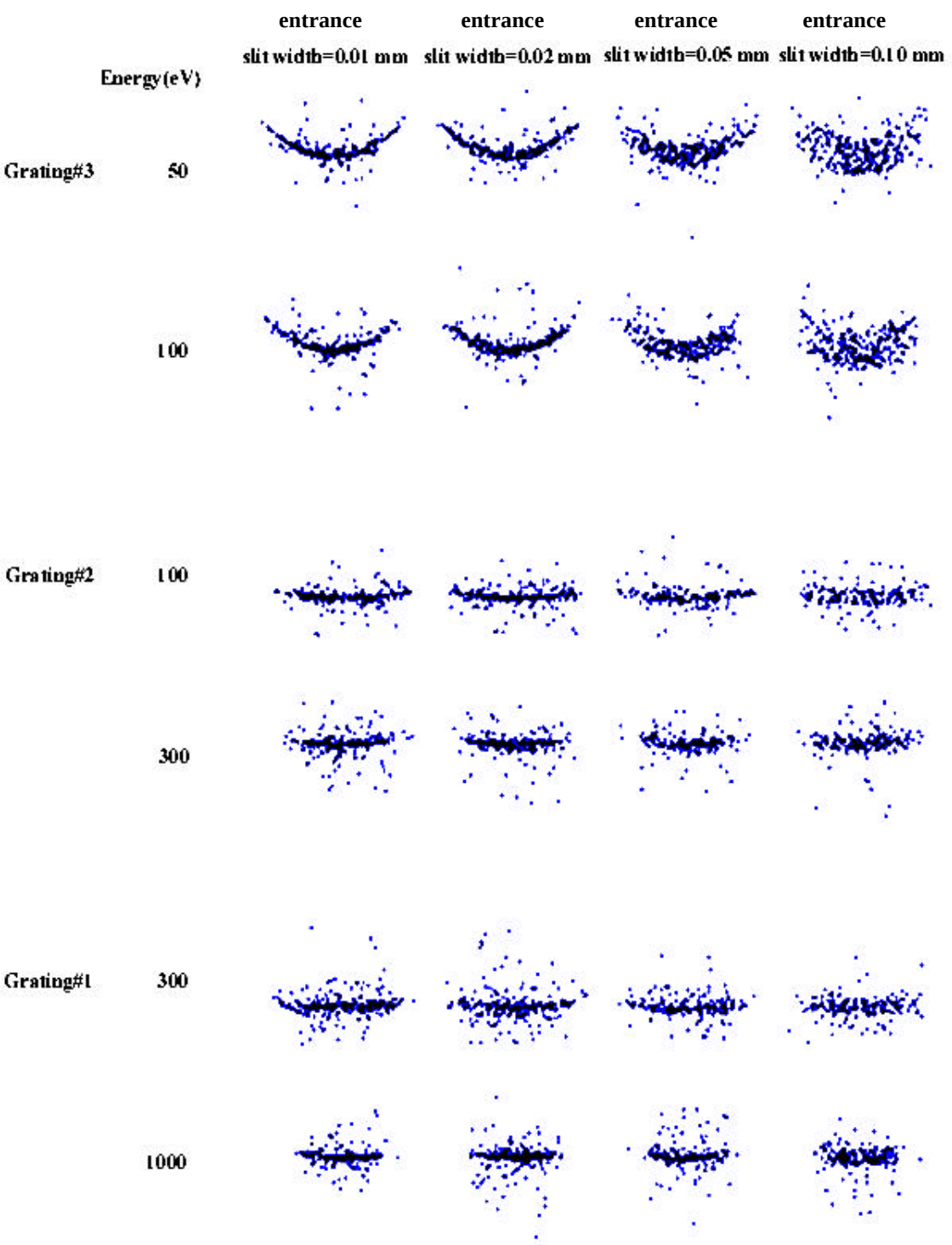

Figure 4.14: *Spot diagram of the image from the spectrometer at difference entrance slit width*

From the Figure 4.14 and the table 4.7 we see that when the entrance slit width is increased the size of the image increases too. The shape of the images are curved because we use the spherical grating in the spectrometer and it is the effect of the spherical shape of the grating. In the case of grating #3 the effects of the aberrations on the image can be seen very clearly. This indicates that by using aberration corrected gratings one can obtain better resolution from the spectrometer.

4.3 Comparison of Resolution Obtained Using Analytical Calculation and Ray Tracing

In this topic we will compare the results of the resolution that we obtained from the calculation with the resolution that we obtain from ray tracing simulation. The resolution from the calculation and from the simulation change in the similar manner. It is observed that the resolution from the simulation is more than the resolution from the calculation. This is expected because the simulation by ray tracing is an approximation of the real time situation where as the empirical formulation is under first order approximation. Thus the results from the simulation is close to the actual case and are accepted in the evaluation.

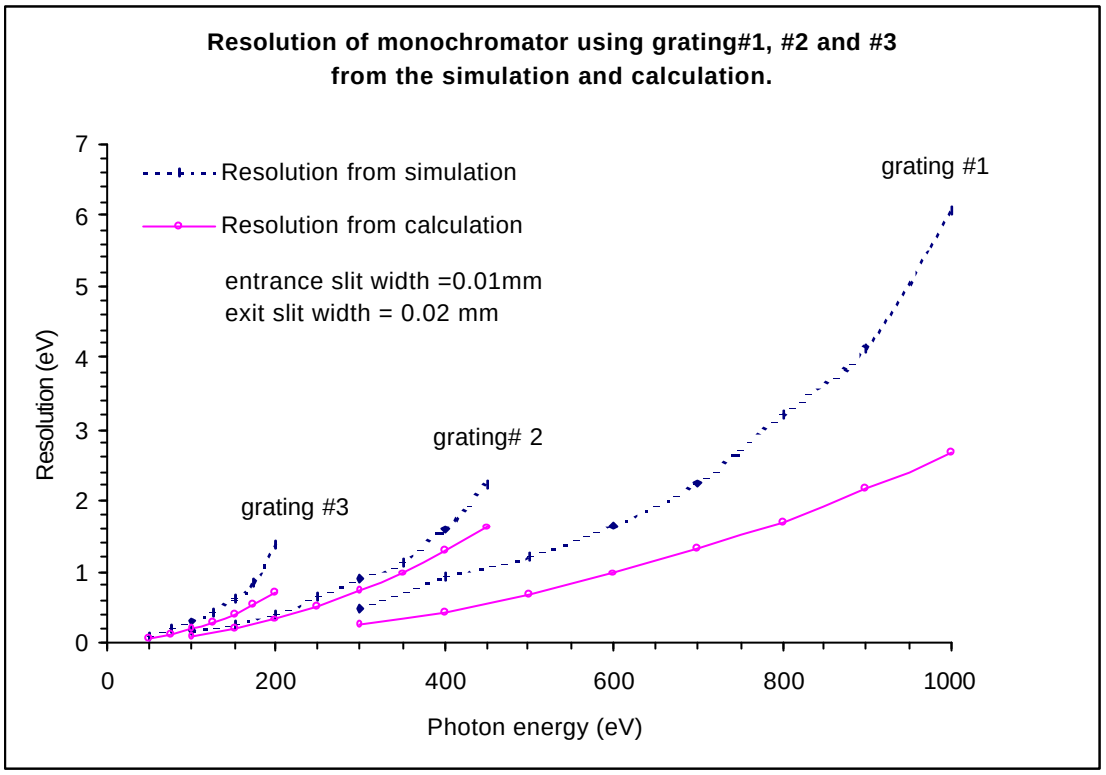

Figure 4.15 : *The comparison of the resolution from the calculation with the resolution from the simulation. The entrance slit width is equal 0.01 mm and exit slit is equal 0.02 mm.*

Chapter V

Conclusions and Future Scope

To fulfil the motivation of designing a high resolving power soft X-ray emission spectrometer with compatable or better performance than the existing commercial one, a detailed optical evaluation is carried out. This evaluation is performed in many steps. Start with using the design criteria such as energy range, resolving power, flux and size and the availability of optical components, the optical parameters of the spectrometer required were evaluated. In the second step the first order evaluations of the spectrometer for efficiency, transmission and resolution were performed using analytical equations. In the third stage, by using the optical parameters, the detailed evaluation of the imaging characteristics of the optics of the spectrometer was performed by means of exact ray tracing. The methodology followed for the optical design evaluation and the results obtained are presented in this thesis.

The spectrometer chosen to serve the requirement of high resolution uses Rowland circle geometry. The reasons for choosing this geometry compared to other geometries are: 1. High transmission 2. High resolution 3. Short space requirement.

The parameters of the spectrometer using three gratings is analyzed as described in the earlier paragraph. The results obtained from this evaluation indicate the following theoretical performance from the design of the soft x-ray spectrometer:

1. The spectrometer is useful for operation over an energy range of 50 – 1000 eV with three spherical gratings.
2. The average transmission efficiencies of the spectrometer while it is operating at highest resolution using three gratings over the energy ranges 50 – 200 eV, 100 – 450 eV and 300 – 1000 eV are 0.1374, 0.1065 and 0.0443 respectively.

3. The average resolving powers (best) of the spectrometer while it is operating at highest resolution using three gratings over the energy ranges 50 – 200 eV, 100 – 450 eV and 300 – 1000 eV are 446.206, 403.738 and 316.032 respectively.
4. The physical size of the optical configuration containing the gratings, slits and the detector is 820 mm approximately.

The future scope of this work can be summarized as:

1. To evaluate the performances of the spectrometer further to see the effects of the slope error and RMS roughness of the surface gratings on the resolution performance.
2. To make a detailed evaluation of mechanical aspects of the construction of the spectrometer to explore the possibility of construction of the spectrometer with the available technology within Thailand.

REFERENCES

References

Aberg, T., and Crasemann, B. (1994). **X-ray Resonant Scattering**. Amsterdam: Elsevier.

Adams, J., Manley, and B.W. (1966), IEEE Trans. **Nucl. Sci**. 13: 88.

Born, M., and Wolf, E. (1980). **Principles of optics.** Oxford: Pergamon Press.

Brown, F. C., Stott, B.P., and Hulbert, R. L. (1986). **Nucl. Instrum. Methods**. A2 (46): 278.

Butorin, S.M., Guo, J.-H., Wassdahl, N., Bray, G. (1994). Tunable excitation x-ray fluorescence spectroscopy in phase analysis of high- Tc superconductors. **J. Phys.: Condensed Matter**, 6 (43): 9267- 74.

Butorin, S.M., Guo, J.-H., Wassdahl, N., Skytt, P. (1995). Electronic Structure of Bi2Sr2CaCu2O8+Delta and T12Ba2CaCu2O8: Near-O-1s-threshold excitation x-ray fluorescence studies. **Phys. Rev. B (Condensed Matter)**, 51 (17): 11915-23.

Carlisle. J.A., Terminello, L.J., Hudson, E.A., and Perera, R.C.C. (1995). Characterization of buried thin films with resonant soft x-ray fluorescence. **Appl. Phys. Lett**. 67 (1): 34.

Codling, K., Mitchell, P. (1970). **J. Phys. E: Sci. Instrum**. 3:685-689.

Dietz, E.F., Braun, W., Bradshaw, A. M. and Johnson, R. L. (1985). **Nucl. Instrum. Methods** A239: 359.

Fabian, D. J. (1968). **Soft X-ray Band Structure**. London: Academic Press.

Fabian, D. J., and Watson, L. M. (1973). **Band Structure Spectroscopy of Metals and Alloys.** London: Academic Press.

Gel'mukhanov, F., and Agren, H. (1994). Channel interference in resonance elastic x-ray scattering. **Phys. Rev. A**, 50 (2A): 1129.

Gel'mukhanov, F., and Agren, H.; (1994). Resonant inelastic x-ray scattering with symmetry-selective excitation. **Phys. Rev. A**, 49 (6): 4378.

Greiner, H., and Schaffer, E. (1957). **Optik**. 14: 263.

Guo, J.-H., Butorin, S.M., Wassdahl, N., and Skytt, P.(1994). Electronic structure of La2-xSrxCuO4 studied by soft-x-ray fluorescence spectroscopy with tunable excitation. **Phys. Rev. B (Condensed Matter)**, 49 (2): 1376-80.

Guo, J.-H., Wassdahl, N., Skytt, P., and Butorin, S. (1993). Electronic structure of La2-xSrxCuO4 studied by resonant soft X-ray fluorescence spectroscopy. **J. Phys. Chem. Solids**. 54 (10): 1203-6.

Henke, B.L., Lee, P., Tanska, T.J., Shimabukuro, R., and Fulikawa, B.K. (1982). **Data Nucl. Data Table2**.

Himpsd, F. J., Jugnet, Y., Eastman, D. E., Donclon, J. J., Grumm, D., Landgren, G., Marx, A.,Morar, J. F., Oden, C., Poilak, R. A., and Schnair, J. (1984). **Nucl. Instrum. Methods**. 222: 107.

Howells, M. R. (1980). **Nucl. Instrum. Methods**. 177: 127.

Howells, M.R. (1980). Plane grating monochromators for synchrotron radiation. **Nucl. Instr. and Meth**. 177: 127-139.

Hunter, W.R. (1985). Measurement of optical constants in vacuum ultraviolet spectral region. **Handbook of optical constants of solids**. New York: Palik Academic.

Ishiguro, E., et.al. (1989). Constant Deviation Monochromator for the range 100 Å<1 <1000 Å. **Rev. Sci. Instrum**. 60: 2105.

Jenkins, F.A., and White, H.E. (1976). **Fundamentals of optics**. 4th edition. New York: McGraw-Hill.

Klaffky, R.W., Howells, M.R., Williams, G.P., Takacs, P.Z., and Godel, J.B. (1982). **Nucl. Instrum. Methods.** 195: 155.

Michette, A.G., Buckley, C.J. (1993). **X-Ray Science and Technology**. Bristol: Institute of Physics Publishing.

Namioka, T. (1954). **Sci. Light.** 3: 15.

Nilsson,A., Bennich,P.,Will, T., and Wassdahl, N.(1995). Direct probing of the adsorbate-substrate chemical bond using angle-dependent x-ray-emission spectroscopy. **Phys. Rev. B (Condensed Matter)**, 51 (15) :10244-7.

Nilsson, P.O., Kanski, J., Thordson, J.V., and Andersson, T.G., (1995). Electronic structure of buried Si layers in GaAs(001) as studied by soft-x-ray emission. **Phys. Rev. B (Condensed Matter)**, 52 (12): 8643-5.

Noda, H., Namioka, T., and Seya, M. (1974). Geometric Theory of grating. **J. Opt. Soc.** Am.64:1031-1036.

Nordgren, E.J. (1996). Soft X-ray emission spectroscopy in the nineties. **J. Electron Spectroscopy and Related Phenomena**. 78 (25): 25-30.

Nordgren, J., Bray, G., Cramm, S., Nyholm, R., Rubensson, J.-E., and Wassdahl N. (1989). Soft x-ray fluorescence spectroscopy. **Rev. Sci. Instrum**. (60) 7: 1690-1696.

Osgood, T. H. (1933). **Phys. Rev**. 44: 517.

Parratt, L. G. (1959). **Rev. Mod. Phys**. 31 616.

Peatman, W.B. (1997). **Gratings, mirrors and slits beamline design for soft X-ray synchrotron radiation source.** Amsterdam: Gordon and Science Publishers.

Perera, R.C.C., Zhang, C.H., Calicott, T.A., and Ederer, D.L. (1989). Electronic bonding of buried interfaces determined by soft x-ray emission spectroscopy. **J. Appl. Phys**. 66 (8): 3676.

Petersen, H. (1982). **Opt. Commun**. 40: 402.

Rehn, V., Baer, A.D., Stanford, J.L., Kayser, D.S., and Jones, V.O. (1974). **Vacuum Ultraviolet Radiation Physics.** Brunschweig: Pergamon-Vieweg.

Rowland, H.A. (1982,1983). The concave diffraction grating. **Philosophical Magazine**, 13: 469-474. Ibid 16: 197-202.

Rubensson, J.-E., Wassdahl, N., Bray, G., Rindstedt, J. (1988). **Phys. Rev. Lett**. 60: 1759.

Saile, V., (1978). **Nucl. Instr. Methods**.(152): 59-67.

Samson, J.A.R. (1967). **Techniques of vacuum ultraviolet spectroscopy** New York: Wiley.

Schäfers, F. (1996). **"RAY" the BESSY Raytrace program to calculate synchrotron radiation beamlines**. BESSY, Berlin. BESSY TB Nr. 202/96.

Schäfers, F., and Krumrey, M. (1996). **"REFLEC" A Program to calculate VUV/ X-Ray optical elements and synchrotron radiation beamlines.** BESSY, Berlin. BESSY TB. Nr. 201/96.

Senf, F., Eggenstein, F., and Peatman, W.B. (1992). Simple constant length Rowland circle monochromators for undulator Radiation. **Rev. Sci. Instrum**. 63:1326-1329.

Senf, F. Lammert, H., Flechsig, U., Zeschke, T., Peatman, W.B., (1995). Precision demanded of Rowland circle monochromator.Its Realisation. **Rev. Sci. Instrum.** 66: 2154-2156.

Seya, M. (1952). **Sci.Light.** 2: 8.

Siegbahn, M. (1937). **Ergebn. Exakt. Naturw**. 16: 104.

Skinner, H. W. B. (1940). **Phil. Trans. Roy. Soc. Lon., Ser**. 239: 95.

Skytt, P., Glans, P., Guo, J, and Gunnelin, K. (1996). Quenching of Symmetry Breaking in Resonant Inelastic X-Ray Scattering by Detuned Excitation. **Phys. Rev. Lett**., vol. 77 (25): 5035.

Songsiriritthigul, P., Pairsuwan, W., Jearanaikoon, S. and Ishii, T. (1999). Siam photon source. **Suranaree J. Sci. Technol.** 6 (1): 22-31.

Southworth, 5., Lindle, D.W., Meyery R., and Cowan, P.L (1991). Anisotropy of polarized x-ray emission from molecules. **Phys. Rev. Lett**. 67 (9): 1098.

Tillborg, H., Nilsson, A., Wiell, T., and Wassdahl, N. (1993). Electronic structure of atomic oxygen absorbed on Ni(100) and Cu(100) studied by soft-x-ray emission and photoelectron spectroscopies. **Phys. Rev. B (Condensed Matter)**. (47) 24: 1646-70.

Tomboulian, H. (1957). **Hanbuch der Physik**. 30. Berlin: Springer-Veriag

Warwick, T., Heimann, P., Mossessain, D., and Padniore**,** H. (1995**) Rev. Sci. Instrum**., 66: 2037.

Wassdahl, N., Nilsson, A., Wiell, T., and Tillborg, H. (1992). Soft x-ray emission studies of adsorbates. **Phys. Rev. Lett**. 69 (5): 812-815.

Wiell, T. (1995). **Soft x-ray emission spectroscopy applied to adsorbates and interfaces**. Ph.D. Thesis, Uppsala University.

Williams, G.P. (1992). **Monochromator System. Synchrotron radiation Research: Advances in Surface and Interface Science**, (2). New York: Issues and Technology.

Williams, R.H., Srivastava, R.H., and MeGoven, I.T. (1980). **Rep. Prog. Phys**. (43): 1357.

APPENDICES

Appendix-1

Synchrotron Radiation

Accelerated charge particles emit electromagnetic radiation. Moving electrons or positrons with relativistic velocities accelerated in magnetic fields emit synchrotron radiation, also called as magnetic bremsstrahlung. The outstanding properties of synchrotron radiation make it an indispensable tool in modern day scientific research. They are

1. **Continuum spectrum:** Synchrotron radiation has a broad continuous spectrum spanning over a wide energy range from the far infrared to x-rays. The spectrum of undulator is comprised of a series of narrow emission bands. By changing the strength of the magnetic field, the locations the band are shifted smoothly and continuously.

2. Extremely high intensities: The intensity of synchrotron radiation is very high. In the case of light from an undulator, the peak intensity is several orders of magnitude higher than that of light coming out from an ordinary bending section.

3. High degree of collimation: Synchrotron radiation has a very low divergence. It is emitted into a very narrow cone tangential to the charged particle trajectory. Along with the very high intensity, this makes the brilliance very high, since the beam size is very samll. In case of an undulator, the charged particle trajectory is confined in a narrow area along the undulator axis and the consequent interference effect makes the brilliance far much higher

4. **The time structure:** The time structure of synchrotron radiation has a form of the repetition of a very short pulse, less than few picoseconds. If measurements are made with low time resolution, the time structure is seemingly such that the light intensity does not fluctuate in time.

5. Quantitatively known characteristics: The spectral brilliance can be completely determined theoretically. Thus synchrotron radiation is capable of serving as a light intensity standard in the region from the vacuum ultraviolet to x-rays.

6. Polarization: Synchrotron radiation from bending section is predominately polarised with the electric vector parallel to the plane of the charged particle orbit. The development of insertion devices, such as helical undulator, can produce circular-polarised synchrotron radiation.

7. Clean environment: The light source operated at 10^{-10} Torr pressure making a clean source and practically free from contamination.

These properties make synchrotron radiation sources as unique ones compared to the conventional sources like halogen lamps, plasma sources and lasers. By using periodic accelerations induced by periodic or helical magnets such as wigglers and undulators it has been proved that it is possible increase the intensity or modify the characteristics of the synchrotron radiation emitted by the relativistic electrons. Such devices with increased complexity are being installed day after day to have light sources with tailor-made characteristics. The aim of this research and development of synchrotron radiation sources is because of the impact these sources have been creating over the last few decades and the increases in demand of sources for specific application. This demand is not only in basic and applied research in Sciences, Engineering and Medicine but also in the research and development of the required application tools in Industry.

Appendix-2

A sample session for Ray tracing using RAY program.

```
*********************************************************************

                        WELCOME TO

                          R  A  Y

                THE BESSY RAYTRACE PROGRAM

                    Version 24.1 of SEPT 2, 1999

                  Franz Schaefers,  BESSY GmbH

                  Lentzeallee 100, D-14195 BERLIN

                      Tel. +49-(0)30-82 004-162

                          FAX              -149

                    e-mail: schaefers@bessy.de

*********************************************************************

  Technical Report available (BESSY-TB 202/96)
  incl. diffraction on rectangular slits   FS 28.7.98
  incl. SGM-fix-focus calculation          FS 25.2.99

                          <RETURN>

(1)  USE PARAMETER FILE ?          (Y/N)              [  YES  ] :

(2)  Filename ? (without extension)      [sxs3-10-20-50            ] :

       reading FILE ***.RAY24 of RAY-Version 24

(3)  CHANGE ANY PARAMETERS ?       (Y/N)        [   NO  ] : y

     CHANGE ANY PARAMETERS ?       (Y/N)        [   NO  ] : y

     Which TERMINAL are you using?

     - X11                                 = 3
```

VMS,UNIX

PC, X-Server software

- TEKTRONIX 4014 = 5

VMS,UNIX : Xterm

PC : KEAterm

- NO GRAPHIC (BATCH-JOB) = 6

- HELP = 9

- EXIT =99 [3] : 6

HARDCOPY ON:

- cancel/ignore (no hardcopy) = 0

- POSTSCRIPT (PS)-PRINTERS:

(4) How many RAYS to be calculated ? [3000000.] :

Specify the SOURCE:

MA__trix (hard edge and angles)

PO__int (hard/soft edge and angles)

PI__xel (hard edge and angles)

CI__rcle (hard edge and angles)

DI__pole (soft edge, hard hor. angle)

WI__ggler (soft edge)

WU__Wiggler/Undulator (soft edge, hard angles)

HU__Helical double Undulator (soft edge, angles)

UF__Undulator-File (output from WAVE or SMUT)

HF__Helical double Undulator-File

FI__le (Source Data-File with X,Y,Z,PHI,CHI)

(4) [po] :

(5) New source parameters ? (Y/N) [NO] : y

(6) Source WIDTH ?

(<0:hard edge, >0:gauss.(sigma) [0.200000 mm] :

(7) Source HEIGHT ?

(<0:hard edge, >0:gauss.(sigma) [0.200000 mm] :

(8) Source DEPTH (hard edge) ? [0.0001 mm] :

(9) Horiz. DIVERGENCE ?

(<0:hard edge, >0:gauss.(sigma) [30.000 mrad] :

(30.00000 mrad: 1.718873 deg/ 6187.944 sec)

(10) Vertical DIVERGENCE ?

(<0:hard edge, >0:gauss.(sigma) [30.000 mrad] :

(30.00000 mrad: 1.718873 deg/ 6187.944 sec)

(11) Horizontal (x) MISALIGNMENT ? [0.000 mrad] :

(12) Vertical (y) MISALIGNMENT ? [0.000 mrad] :

(13) Horizontal (x) OFFSET ? [0.00000 mm] :

(14) Vertical (y) OFFSET ? [0.00000 mm] :

(15) Photon ENERGY ? [50.000 eV] :

(Photon wavelength: 24.7970 nm)

(16) Energy-spread Delta-E ?

(<0: white band, >0: 3 Energies) [-0.31700 eV] :

(17) LINEAR polarization (S1/S0) ?

(e-vector hor.:S1=1, vert.:S1=-1) [1.000] :

(18) LINEAR polarization (S2/S0) ?

(e-vector 45 deg. w.r.t. S1) [0.000] :

(19) CIRCULAR polarization (S3/S0) ?

(sigma+, left-handed CP: S3 > 0) [0.000] :

(TOTAL polarization: 1.000)

(20) SOURCE PARAMETERS O.K. ? (Y/N) [YES] :

(21) How many OPTICAL ELEMENTS ? (0-10) [3] :

Specify the 1. OPTICAL ELEMENT

SL__it

FO__il

ZO__neplate

PM__plane mirror

CY__cylinder

CO__ne

SP__here

TO__roid

EL__lipsoid

PA__raboloid

DI__aboloid

PG__plane grating

SG__spherical grating

TG__toroidal grating

CR__ystal

CC__ylindrical crystal

(22) [SL] :

(23) NEW ELEMENT parameters ? (Y/N) [NO] : y

(24) Total WIDTH (x-dir.) (<0: R-min) [1.5000 mm] :

(25) Total HEIGHT (y-dir.) (<0: R-max) [0.0100 mm] :

(26) DISTANCE to preceding element/source [30.000 mm] :

(27) MISALIGNMENT or SLOPE ERRORS ? (Y/N) [N] :

(28) OPT.ELT. PARAMETERS O.K. ? (Y/N) [YES] :

Specify the 2. OPTICAL ELEMENT

SL__it

FO__il

ZO__neplate

PM__plane mirror

CY__cylinder

CO__ne

SP__here

TO__roid

EL__lipsoid

PA__raboloid

DI__aboloid

PG__plane grating

SG__spherical grating

TG__toroidal grating

CR__ystal

CC__ylindrical crystal

(29) [SG] :

(30) NEW ELEMENT parameters ? (Y/N) [NO] : y

(31) Total WIDTH (x-dir.) (<0: R-min) [50.0000 mm] :

(32) Total LENGTH (z-dir.) (<0: R-max) [200.0000 mm] :

(33) Diffraction ANGLE:

> 0: ALPHA-BETA (2THETA) f. const. deviation mount

<=0: ALPHA f. const. incidence angle mount

700: SGM - fix-focus

(34) [-84.6000 deg] :

(35) ENTRANCE ARM length [282.4 mm] :

(36) EXIT ARM Length [460.90 mm] :

(37) LINE DENSITY (<0 : VLS-grating) [300.00l/mm] :

(38) ORDER of diffraction

(>0: inside order, alpha > beta) [1.] :

(calculated alpha,beta = 84.6000 -81.1606 deg)

(39) Normal INCIDENCE ANGLE alpha [84.6000 deg] :

(40) Normal INCIDENCE ANGLE beta [-81.1606 deg] :

(41) DISTANCE to preceding element/source [282.400 mm] :

(42) AZIMUTHAL ANGLE

rotation in x-y plane, around z-(light) direction

right-hand rule: x-->y (e.g. for 1st opt. elt.):

deviation up (down-)wards:0(180)deg.

... right (left) 90(270) [0.000 deg] :

(43) Name of Coating/Foil/ Crystal [Au] :

(calculated R = 3000.1 mm)

(44) Long RADIUS R (infinity: 0) [3000. mm] :

(45) PROFILE (1:blaze 2:sinus 3:laminar)

(4:unknown, do NOT calc. Efficiency [1.] :

(46) BLAZE ANGLE [0.97 deg] :

ASPECT ANGLE (ideal grating: 90 deg.)

realistic:blaze:90-179,lamin:1-90 deg [90.00 degr.] :

(47) MISALIGNMENT or SLOPE ERRORS ? (Y/N) [N] :

OPT.ELT. PARAMETERS O.K. ? (Y/N) [YES] :

(48) Grating EFFICIENCY: 50.0000000000000 eV 84.6000000000000 deg:

Rs: 0.298278907465628 Rp: 0.261713776710315

Specify the 3. OPTICAL ELEMENT

SL__it

FO__il

ZO__neplate

PM__plane mirror

CY__cylinder

CO__ne

SP__here

TO__roid

EL__lipsoid

PA__raboloid

DI__aboloid

PG__plane grating

SG__spherical grating

TG__toroidal grating

CR__ystal

CC__ylindrical crystal

(49) [SL] :

(50) NEW ELEMENT parameters ? (Y/N) [NO] : y

(51) Total WIDTH (x-dir.) (<0: R-min) [50.0000 mm] :

(52) Total HEIGHT (y-dir.) (<0: R-max) [0.0500 mm] :

(53) DISTANCE to preceding element/source [460.900 mm] :

(54) MISALIGNMENT or SLOPE ERRORS ? (Y/N) [N] :

OPT.ELT. PARAMETERS O.K. ? (Y/N) [YES] :

(55) Display BEAM-WIDTH (find FOCUS-position)? [N] :

(56) How many IMAGE PLANES ? (1-3) [1] :

(57) DISTANCE of 1. IMAGE PLANE fr. last OE [0.000 mm] :

(58) STORE PARAMETERS ? (Y/N) [NO] :

(59) START CALCULATIONS ? (Y/N/ E_xit) [YES] :

```
raytracing test loop #     500 (successful:     0)
raytracing test loop #    1000 (successful:     0)
raytracing test loop #    1500 (successful:     0)
        :                    :
        :                    :
raytracing test loop #   98500 (successful:    29)
raytracing test loop #   99000 (successful:    31)
raytracing test loop #   99500 (successful:    31)
```

(60) POSITION LIMITS (in mm) at Source (x-y),
Opt. Elements (x-z), and Image Planes (x-y)

No	Name	Xmin	Xmax	Y(Z)min	Y(Z)max
1:	PO	-0.5998	0.5995	-0.5999	0.5994
2:	SL	-0.7486	0.7495	-0.0050	0.0050
3:	SG	-11.5681	14.0214	-43.0926	50.8560
4:	SL	-19.5749	21.7120	-0.0240	0.0240
5:	IM	-19.5749	21.7120	-0.0240	0.0240

No	Name	E_min	E_max
1:	PO	49.8415	50.1585
2:	SL	49.8415	50.1582
3:	SG	49.8415	50.1582
4:	SL	49.8830	50.1491
5:	IM	49.8830	50.1491

(61) ANGULAR LIMITS horizontal and vertical (degree)

No	Name	PHImin	PHImax	PSImin	PSImax
1:	PO	-5.1503	5.1511	-5.1499	5.1556
2:	SL	-2.1936	2.3886	-0.8965	0.8975
3:	SG	-2.1388	2.3219	80.0856	81.9020
4:	SL	-1.4319	1.6033	-0.6676	1.0129
5:	IM	-1.4319	1.6033	-0.6676	1.0129

88 rays successful (31 reflected) out of 99500 rays

(62) DISTANCE of 1. IMAGE PLANE fr. last OE[0.000 mm] :

(63) START WITH RAYTRACING ? (Y/N/ E_xit) [YES] :

raytracing at ray number: 5000. (CTRL/H: finish, CTRL/K: stop)
raytracing at ray number: 10000. (CTRL/H: finish, CTRL/K: stop)
raytracing at ray number: 15000. (CTRL/H: finish, CTRL/K: stop)
: :
: :
raytracing at ray number: 2990000. (CTRL/H: finish, CTRL/K: stop)
raytracing at ray number: 2995000. (CTRL/H: finish, CTRL/K: stop)
raytracing at ray number: 3000000. (CTRL/H: finish, CTRL/K: stop)

---------- CALCULATIONS DONE ----------
---

(64)

No	Name	N_geometric	N_reflected	Max. Flux density (N/mm**2)	Flux (N/s/0.1A/ 0.63%BW)
1:	PO	3000000.	3000000.	0.4229D+01	0.1000D+01
2:	SL	7621.	7621.	0.1344D+01	0.2540D-02
3:	SG	7621.	2267.	0.3712D-05	0.7557D-03
4:	SL	2562.	752.	0.1480D-02	0.2507D-03
5:	IM	2562.	752.	0.1480D-02	0.2507D-03

No	Name	Stokes-Vector:	S1/S0	S2/S0	S3/S0
1:	po		1.000	0.000	0.000
2:	sl		1.000	0.000	0.000
3:	sg		1.000	0.000	0.000
4:	sl		1.000	0.000	0.000
5:	IM		1.000	0.000	0.000

(65) Display source ? [NO] :

(66) Display 1. optical element (sl) ? [NO] :

(67) Display 2. optical element (sg) ? [NO] :

(68) Display 3. optical element (sl) ? [NO] : y

(69) Display point-diagram (footprint) ? [NO] :

(70) Display energy distribution ? [NO] : y

Width: 0.1261 eV, Center: 50.028 eV

Abszissa: min ? [49.86973] :

... max ? [50.16306] :

Ordinate: min ? [0.00000] :

... max ? [63.00000] :

Header ? [ ] :

%PLT94-F-... PLINIT Device number 99 not allowed.

(71) change scale ? (Y/N) [NO] :

(72) hardcopy ? (Y/N) [NO] :

(73) Store data (#1) ? (Y/N) [NO] :

(74) Display x-z(y) angular distribution ? [NO] :

(75) Display y-z angular distribution ? [NO] :

(76) Display 3-D surface profile ? [NO] :

(77) store all data ? [NO] :

(78) Display 1. image plane ? [NO] :

(79) Repeat graphics (Y/N/ E_xit) ? [NO] : y

(80) Display source ? [NO] :

(81) Display 1. optical element (sl) ? [NO] :

(82) Display 2. optical element (sg) ? [NO] :

(83) Display 3. optical element (sl) ? [NO] : y

(84) Display point-diagram (footprint) ? [NO] : y

Abszissa: min ? [-29.29453] :

... max ? [28.73240] :

Ordinate: min ? [-0.02988] :

... max ? [0.02990] :

Header ? [ ] :

%PLT94-F-... PLINIT Device number 99 not allowed.

Width(x): 25.598 mm, center: 0.036 mm

Width(y): 0.036 mm, center: 0.000 mm

Phot./s/0.1A/ 30.0mrad/0.634%BW: .2507D-03

(85) change scale ? (Y/N) [NO] :

(86) hardcopy ? (Y/N) [NO] :

(87) Store Footprint data ? (Y/N) [NO] :

(88) Display energy distribution ? [NO] :

(89) Display x-z(y) angular distribution ? [NO] :

(90) Display y-z angular distribution ? [NO] :

(91) Display 3-D surface profile ? [NO] :

(92) store all data ? [NO] :

(93) Display 1. image plane ? [NO] :

(94) Repeat graphics (Y/N/ E_xit) ? [NO] :

Appendix-3

A sample session using REFLEC program.

```
**************************************************************************
                        WELCOME TO
                        R  E  F  L  E  C
                    a program to calculate
                VUV/X-RAY OPTICAL ELEMENTS
                            and
            SYNCHROTRON RADIATION BEAMLINES
                    Version 21.4 of SEPT/6/1999
                Franz Schaefers,  BESSY GmbH
                and Michael Krumrey, PTB
                Lentzeallee 100, D-14195 BERLIN
                Tel. BESSY-I :+49-(0)30-82004 162
                Tel. PTB/B-II:+49-(0)30-6392 5085
                e-mail: Name@BESSY.DE
**************************************************************************
        - radiation dose in the direct beam (15.4.98 MK)
        - grating calc. for constant incidence angle (7.5.98 FS)
        - new: PO_larimeter f. polarisation analysis (23.6.99 FS)
        - new Henke-tables for Li,Mg,Al,Si,Fe,Mo,Au  (24.6.99 FS)

                                                                <RETURN>

  INFORMATION ABOUT THE PROGRAM ? (Y/N)                 [  NO  ] :

  USE PARAMETER FILE ?          (Y/N)                   [  NO  ] : y
  Filename ? (without extension) [] : test

  CHANGE ANY PARAMETERS ?       (Y/N)                   [  NO  ] : y
  HOW MANY ELEMENTS TO BE CALCULATED (1 - 10)?          [   1  ] :
  NEW PARAMETERS FOR   1. ELEMENT ?                     [  NO  ] : y
```

```
TYPE OF 1. ELEMENT:
      SO__urce
      MI__rror
      GR__ating
      FO__il
      WI__ndow
      CR__ystal
      PO__larimeter
      MA__terial properties
                  [  mi  ] :
START PHOTON ENERGY ?                                  [   20.00 eV  ] : 50
         (wavelength:    24.7970nm)
STOP PHOTON ENERGY ?                                   [  320.00 eV  ] : 1000
          (wavelength:     1.2399nm)
MULTILAYER COATING - NUMBER OF LAYERS
          (<0: including additional top layer)
          (-1: input by SUPERMIRROR.DAT-File)
          (-2: SUPERMIRROR.DAT-File with top layer)
               [       1.  ] :
MIRROR SUBSTRATE (SiO2, ZERODUR,.. )?                  [      Si           ] :
ROUGHNESS of SUBSTRATE or FOIL ?                       [       1.00 nm     ] :
DENSITY   of SUBSTRATE or FOIL ?                       [  2.320 g/cm^3 ] :
MATERIAL  of 1. COATING ?                              [      Au           ] :
THICKNESS of 1. COATING ?                              [      10.00 nm    ] :
ROUGHNESS of 1. COATING ?                              [       1.00 nm    ] :
DENSITY   of 1. COATING ?                              [ 19.300 g/cm^3] :
GRAZING INCIDENCE ANGLE
          or calculate/read angle according to:
          700: SX700 (PM)-focal curve - const. c_ff
          200: SGM       -focal curve (not yet installed)
          300: hv/angle-table from FILE                [  4.0000 deg.] : 1

OPT.ELT. PARAMETERS O.K. ? (Y/N)                       [  YES  ] :
NEW DISPLAY PARAMETERS FOR   1. ELEMENT ?              [   NO  ] :

STORE PARAMETERS ?           (Y/N)                     [   NO  ] :

START CALCULATIONS ?      (Y/N/ E_xit)                 [  YES  ] :
```

```
--------------------------------------------------------------------------
--- REFLEC IS CALCULATING THE          1. ELEMENT ---
--------------------------------------------------------------------------
reading Henke-table for f1,f2: Si.f12h       (30 eV - 30 keV)
 reading Henke-table for f1,f2: Au.f12h     (30 eV - 30 keV)

 --------------------------------------------------------------------------
-------------------------CALCULATIONS DONE ------------------
--------------------------------------------------------------------------

AND NOW ?
        Graphic DISPLAY          (=1)
        HARDCOPY                 (=2)
        WRITE ASCII-data         (=3)
        READ ASCII-file          (=4)
        CHANGE Parameters        (=5)
        BACK to START            (=6)
        EXIT           (=9)      [ 1 ] : 3
Filename (no extension, list on screen:TT) [] :test
REFLEC is writing the  1. curve
DATA are stored in file "test.nem  "
```

Biography

Mr. Narudom Noulkhow was born on August 29, 1975 in Surathani province. He received his Bachelor's Degree in Science (Physics) from Prince of Songkla University in 1997. He continued with his graduate studies in the School of Physics, Institute of Science, Suranaree University of Technology.